ISSN 0002-7014
AMEGHINIANA - 2023 - Volume 60(4): xx–xx

ENHANCED PRIMARY PRODUCTIVITY IN THE BRAZIL MALVINAS CONFLUENCE ZONE DURING THE MIS 3

CECILIA LAPRIDA[1], PAULA B. ALBARRACÍN[1], SILVIA I. ROMERO[2,3,4], RODRIGO S. MARTÍN[1], JOSÉ ISOLA[5], SABINE KASTEN[6,7,8], AND NATALIA GARCÍA CHAPORI[1]

[1]Instituto de Estudios Andinos "Don Pablo Groeber", UBA-CONICET, Facultad de Ciencias Exactas y Naturales, Universidad de Buenos Aires, Ciudad de Buenos Aires, Argentina. *chechulaprida@gmail.com*; *pau.albarracin23@gmail.com*; *rodrigosmartin88@gmail.com*; *natalia.garcia.chapori@gmail.com*

[2]Servicio de Hidrografía Naval, Ciudad de Buenos Aires, Argentina. *sroceano@apexar.com*

[3]Departamento de Ciencias de la Atmósfera y los Océanos, Facultad de Ciencias Exactas y Naturales, Universidad de Buenos Aires, Ciudad de Buenos Aires, Argentina.

[4]Universidad de la Defensa Nacional, Ciudad de Buenos Aires, Argentina.

[5]Instituto de Geología Básica y Aplicada - IGEBA, UBA-CONICET, Facultad de Ciencias Exactas y Naturales, Universidad de Buenos Aires, Ciudad de Buenos Aires, Argentina. *jose.isola91@gmail.com*

[6]Alfred Wegener Institute, Helmholtz Centre for Polar and Marine Research, Bremerhaven, Germany. *sabine.kasten@awi.de*

[7]Faculty of Geosciences, University of Bremen, Bremen, Germany.

[8]MARUM Center for Marine Environmental Sciences, Bremen, Germany.

Abstract. Micropaleontological analyses from the western South Atlantic core AU_Geo02_GC20 (45° 55′ S; 58° 30′ W, 2589 m water depth) revealed changes in the primary productivity and sea surface temperature (SST) during MIS 3 that point to significant changes in the Brazil Malvinas Confluence Zone dynamics. These changes led to a marked increase in the SST and the primary productivity between 44.0–36.1 ka BP, as indicated by the quantitative reconstruction of the subsurface temperature and the high relative abundance of the planktonic foraminifera *Globigerina bulloides* and the eutrophic index. The increase in the SST and the primary productivity could indicate frequent or more persistent southward penetration of subtropical waters over the north Patagonian margin due to a southward extension of the Brazil Current and a weakening of the Malvinas Current. The high primary productivity resulted in the intensive use of phosphate during spring. Conversely, benthic assemblages do not reflect high surface productivity. The dominance of calcareous nannoplankton over diatoms as primary producers, which allows inferring the shoaling of the nutricline and the thermocline, justifies the decoupling between planktonic and benthic communities as a consequence of reduced efficiency of the biological pump. The deposition of the pelagites during the period of enhanced primary productivity indicates a slowing down of the bottom circulation, probably due to a weakening of the Atlantic Meridional Overturning Circulation.

Key words. Paleoceanography. Western South Atlantic. Patagonian Continental Margin. Late Pleistocene. Bentho-pelagic decoupling. Micropaleontology.

Resumen. INCREMENTO DE LA PRODUCTIVIDAD PRIMARIA EN LA ZONA DE CONFLUENCIA BRASIL MALVINAS DURANTE EL ESTADÍO ISOTÓPICO 3. Los análisis micropaleontológicos del testigo AU_Geo02_GC20 (45° 55′ S; 58° 30′ W, 2589 m de profundidad del agua), Atlántico Sudoccidental, revelaron cambios en la productividad primaria y la temperatura del agua superficial (SST) durante el MIS 3 que implican cambios significativos en la dinámica de la Zona de Confluencia Brasil Malvinas. Estos cambios condujeron a un marcado aumento en la SST y en la productividad primaria entre 44 y 36,1 ka AP, como lo indican la reconstrucción cuantitativa de la temperatura sub-superficial, la elevada abundancia relativa del foraminífero planctónico *Globigerina bulloides* y el índice de productividad eutrófica. La alta productividad primaria condujo a un uso intensivo de fosfato durante la primavera. El aumento de la SST y de la productividad primaria podrían indicar una frecuente o más persistente penetración de aguas subtropicales sobre el margen norte patagónico debido a una extensión hacia el sur de la Corriente de Brasil y el concurrente debilitamiento de la Corriente de Malvinas. Por el contrario, los ensambles de foraminíferos bentónicos no reflejan una alta productividad superficial. El dominio de cocolitofóridos sobre diatomeas como productores primarios, que permite inferir la somerización de la nutriclina y la termoclina, justifica el desacople entre las comunidades planctónicas y bentónicas como consecuencia de una menor eficiencia de la bomba biológica. La deposición de pelagitas calcáreas fangosas durante este período de mayor productividad primaria indica una desaceleración de la circulación del fondo, probablemente debido a un debilitamiento de la *Atlantic Meridional Overturning Circulation*.

Palabras clave. Paleoceanografía. Atlántico Sudoccidental. Margen Continental Patagónico. Cuaternario tardío. Desacoplamiento pelágico-bentónico. Micropaleontología.

THERE IS A STRONG LINK between marine primary productivity and climate (*e.g.*, Schneider *et al.*, 2007). Upwelling and highly productive marine systems play an essential role in the marine carbon cycle and atmospheric CO_2 uptake (Hales *et al.*, 2005; Cao *et al.*, 2014) with critical consequences on global (Ciais *et al.*, 2014) and regional climate (Franchito *et*

al., 2008) on different timescales, ranging from interannual to multi-millennial (Friedlingstein, 2015). Climate model simulations have shown that, in a warming climate, primary productivity, as well as particulate organic carbon export production, will probably be reduced (Sarmiento *et al.*, 2004). Thus, the knowledge of changes in the primary productivity of highly productive ocean systems and the subsequent transport of organic matter to the sea floor in different climatic scenarios is essential for carbon cycle modeling, providing a unique opportunity to understand the response of the biological carbon pump to past global climate changes outside the modern climate range for which current models have been developed (Braconnot *et al.*, 2012; Kageyama *et al.*, 2018).

The coasts of Patagonia south of 40° S (Fig. 1) host one of the most productive marine ecosystems of the world ocean (Piola & Falabella, 2009), with marine productivity rates comparable to wind-driven coastal upwelling regions (Gregg *et al.*, 2005). Field and remote sensing data show that streaks of very high chlorophyll-a (**Chl-a**) concentration and phytoplankton are consistently observed from early austral spring to late summer (Romero *et al.*, 2006; Saraceno *et al.*, 2005; Dogliotti *et al.*, 2014). These streaks that extend from 37 to 51° are parallel to the bathymetric contours, showing maximum values in the shelfbreak zone (the limit between the outer shelf and the slope) where satellite-derived surface Chl-a is characterized by a strong annual cycle (García *et al.*, 2004; Romero *et al.*, 2006). During summer, the entire shelfbreak exhibits a band of very high Chl-a related to a strong upwelling. This upwelling brings up nutrients and supports a very high primary productivity (Marrari *et al.*, 2017). A steady alongshore current induces this shelfbreak upwelling in the direction of propagation of coastal trapped waves and the rapid change in the Ekman transport at the shelfbreak (Matano & Palma, 2008; Miller *et al.*, 2011). Offshore the shelfbreak, the Patagonian margin shows higher Chl-a values between the Subantarctic Front (**SAF**) and the Subtropical Front (**STF**) in contrast with the oligotrophic waters of the Subtropical Gyre located northwards, but lower values compared with the Patagonian shelf (Fig. 1). Based on satellite-derived surface Chl-a data and regional oceanography, Longhurst (2006) defined the *Southwest Atlantic Shelves Province*, that comprises the Argentine shelf between 38°–55° S and is characterized by a *very high* Chl-a concentration; and the *South Subtropical Convergence (**SSTC**) Province* that lies across the southern side of the southern subtropical gyres of each ocean basin, between the STF and the SAF. In the South Atlantic, its westernmost margin limits with the Southwest Atlantic Shelves Province, and it is characterized by *high* Chl-a concentrations. Whereas space and time variability in satellite Chl-a concentrations has been extensively studied

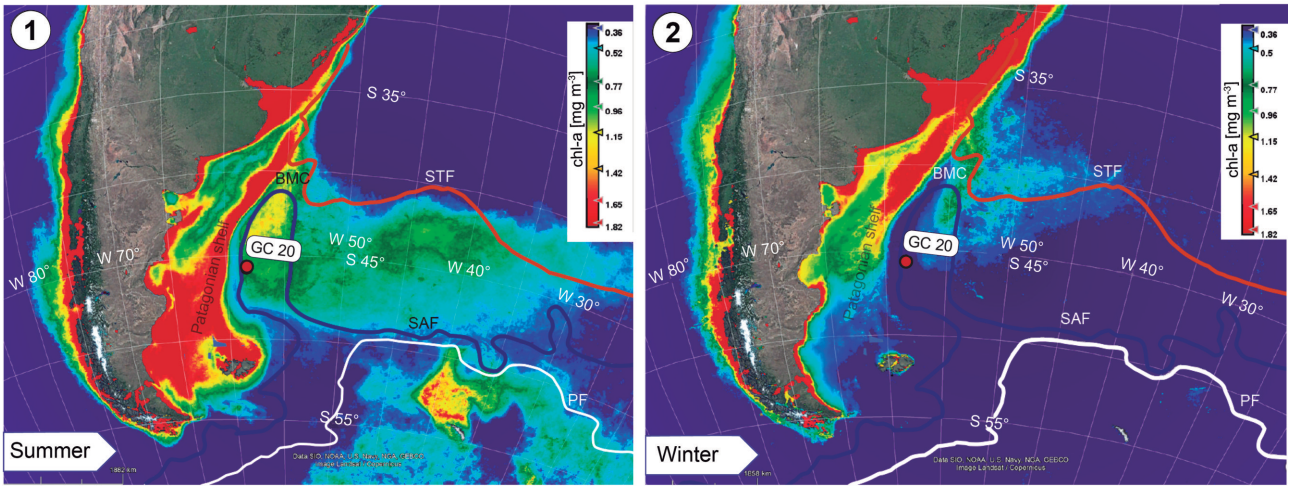

Figure 1. Summer (1) and winter (2) satellite chlorophyll-a (Chl-a) distributions showing the differences at the AU_Geo02_GC20 core position (red dot). Concentrations increase from violet to red, and during summer they are *very high* over the shelf and *high* at the westernmost limit of the South Subtropical Convergence Province under variable influence of the energetic Brazil-Malvinas Confluence Zone. Also drawn are the fronts of the Antarctic Circumpolar Current (Orsi *et al.*, 1995), the Subantarctic Front (**SAF**, blue), the Subtropical Front (**SF**, red), and the Polar Front (**PF**, white). Chl-a data are from Aqua/MODIS Level-3 Binned Version 2018. They correspond to seasonal climatologies (a composite of all of the data collected during a single season for the period 2002-2021, NASA 2018).

for the Southwest Atlantic Shelves Province (Rivas *et al.*, 2006; Romero *et al.*, 2006; Marrari *et al.*, 2017), our knowledge about the long-term variability of the primary productivity of the westernmost margin of the SSTC at the Patagonian margin and the response of the system to long-term climate changes, is still largely unknown.

The Marine Isotope Stage 3 (**MIS 3**) is a relatively warm interval between 57 and 29 ka BP (Lisiecki & Raymo, 2005), an interstadial within the last ice age. The global sea level was 60-90 meters lower-than-present level (Grant *et al.*, 2012). Abrupt climatic changes during this stage were related to changes in the strength of Atlantic Meridional Overturning Circulation (**AMOC**), affecting the interhemispheric heat exchange (Agosta Scarel & Compagnucci, 2016). Despite the increasing number of studies on the past variability and intensity of primary productivity in the western South Atlantic, high-resolution paleoceanographic records from MIS 3 are still scarce. Most studies have mainly focused on changes in the coastal upwelling system off Southern Brazil during the Holocene (*e.g.*, Nagai *et al.*, 2008; Lessa *et al.*, 2014). Primary productivity changes, including the MIS 3, have been published in recent years and assigned to different factors: shifts in the upwelling intensity of South Atlantic Central Water (Portilho-Ramos *et al.*, 2015); the strengthening of the northern intrusion of the Rio de la Plata Plume as a consequence of the shift of the South Westerlies core (Portilho-Ramos *et al.*, 2018); and changes in the intensity of the AMOC (Pereira *et al.*, 2018). In the western South Atlantic, early studies on foraminiferal assemblages focused on Mesozoic and Cenozoic stratigraphy of the Argentine Basin (Basov *et al.*, 1983; Bertels, 1987; Bertels & Núñez, 1989) and the Plio–Pleistocene paleoceanographic evolution (Cusminsky, 1991, 1992, 1994) of the southern Patagonian margin. More recently, studies are mainly focused on the modern distribution of benthic foraminifera in modern marginal marine and shelf environments (Bernasconi & Cusminsky, 2020; Alperín *et al.*, 2011; Bernasconi *et al.*, 2018, 2019) and its use as proxies in Holocene sequences (Bernasconi *et al.*, 2009).

The aforementioned geographical and temporal limitation of paleoceanographic reconstructions hinders our understanding of the long-term variability of marine productivity off the Patagonian margin. The main goal of this study is to fill this gap by reconstructing the primary productivity and surface ocean conditions of the north Patagonian margin during MIS 3 (Fig. 2) by integrating several lines of evidence, including lithology and quantitative studies of both planktonic and benthic foraminifera. We intend to decipher the relative role of western South Atlantic boundary currents on the primary productivity of the Patagonian margin. We hypothesize that during the MIS 3, the primary productivity was enhanced at the western margin of the South Subtropical Convergence Province as a consequence of changes in the position of the Brazil Malvinas Convergence (**BMC**) related to a reinforced Brazil Current and a weakened Malvinas Current. Other factors, such as the sea level and the role of the South Westerly Winds (**SWW**), are also discussed.

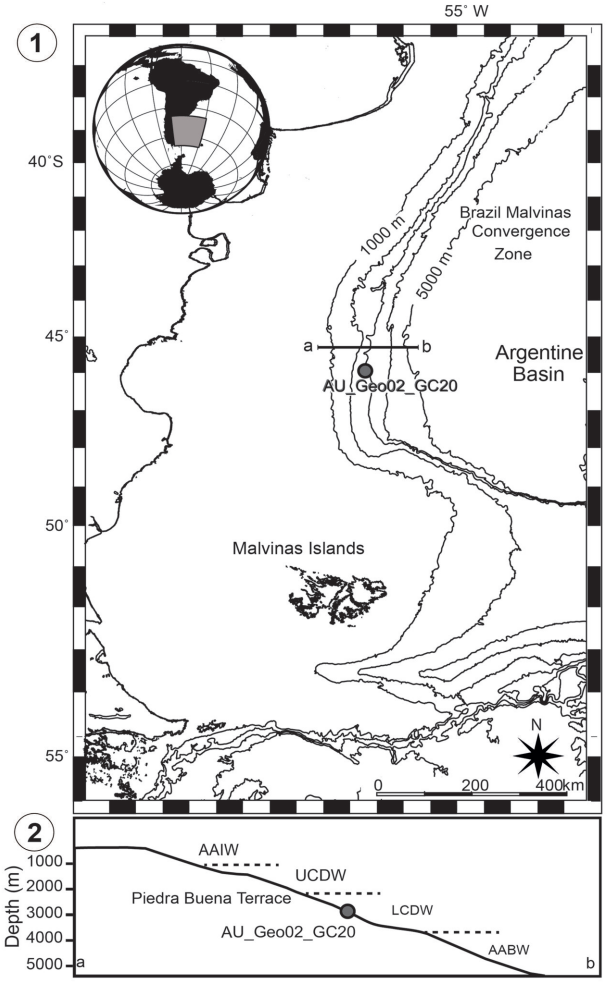

Figure 2. 1) The Argentine Continental Margin and the location of the core studied. 2) Schematic hydrographic section showing the main intermediate and deep water masses that interact with the seafloor at 45°S: **AAIW**: Antarctic Intermediate Water; **UCDW**: Upper Circumpolar Deep Water; **LCDW**: Lower Circumpolar Deep Water; **AABW**: Antarctic Bottom Water. (Modified after Isola *et al.*, 2021).

Abbreviations. AABW, Antartic Bottom Water; **AAIW,** Antarctic Intermediate Water; **ACC,** Antarctic Circumpolar Current; **AMOC,** Atlantic Meridional Overturning Circulation; **aph443,** absorption coefficient of phytoplankton at 443 nm; **AR,** Accumulation Rate; **BC,** Brazil Current. **BCO,** BC overshoot; **BFAR,** Benthic Foraminifera accumulation rate; **BFN,** Benthic Foraminifera number; **BMC,** Brazil Malvinas Confluence; **BMCZ,** Brazil Malvinas Confluence Zone; **CCA,** Canonical Correspondence Analysis; **CDW,** Circumpolar Deep Water; **Chl-a,** chlorophyll-a; **DBD,** Dry bulk density; **DCA,** Detrended correspondence analysis; **EKE,** Eddy kinetic energy; **FPI,** Foraminiferal productivity Index; **LCDW,** Lower Circumpolar Deep Water; **LOI,** Loss-on-ignition; **LSR,** Linear sedimentation rates; **MC,** Malvinas Current; **MCR,** Malvinas Current Retroflection; **MIS 3,** Marine Isotope Stage 3; **ML,** Maximum likelihood; **MUW,** Malvinas Upper Water; **NADW,** North Atlantic Deep Water; **PCA,** Principal component analysis; **PCM,** Patagonian continental margin; **PFN,** Planktonic Foraminifera number; **Phosspring,** spring phosphate; **POC,** Particulate organic matter; **RMSEP,** Root-Mean-Square error of prediction; **SAF,** Subantarctic Front; **SEC,** South Equatorial Current; **SSAW,** Surface Subantarctic Water; **SST,** Sea surface temperature; **SSTC,** South Subtropical Convergence; **STF,** Subtropical Front; **SWW,** South westerly winds; **TC,** Total Carbon; **UCDW,** Upper Circumpolar Deep Water; **WA,** Weighted averaging; **WA-PLS,** Weighted averaging-Partial least squares.

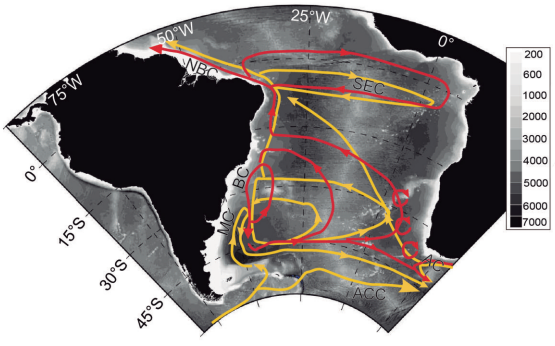

Figure 3. Scheme of the upper and intermediate components of the current South Atlantic large-scale circulation. The color-coded paths represent the flow at both different vertical levels: upper (Tropical Water; South Atlantic Central Water, red) and intermediate (Antarctic Intermediate Water and Upper Circumpolar Deep Water, yellow). Deep and abyssal components are not shown. The names of the main currents are indicated: Agulhas Current (**AC**), Antarctic Circumpolar Current (**ACC**), Brazil Current (**BC**), Malvinas Current (**MC**), North Brazil Current (**NBC**), and South Equatorial Current (**SEC**). Adapted from Valla *et al.* (2018).

OCEANOGRAPHIC AND GEOLOGICAL SETTINGS

Oceanographic settings

In the South Atlantic Ocean, the anticyclonic upper circulation pattern, referred to as the Subtropical Gyre, is induced by the interplay between the low latitude easterlies and mid-latitude South westerly winds (**SWW**). The western limb of the Subtropical Gyre, the Brazil Current (**BC**), carries warm and salty waters polewards along the continental slope of Brazil, Uruguay, and northern Argentina (Fig. 3). The BC originates between 10°–15°S along the continental slope of South America through a bifurcation of the westward flowing South Equatorial Current (**SEC**). The northern branch of the SEC, the North Brazil Current, represents a loss of upper layer mass from the South Atlantic to the North Atlantic. The southern branch of the SEC forms the BC (Piola & Matano, 2001). Near 38°S, the BC collides with the cold and relatively fresh Malvinas Current (**MC**). The MC originates in the Drake Passage, where the steep topography forces the northernmost branch of the Antarctic Circumpolar Current (**ACC**) to turn northwards. Along the western boundary of the Argentine Basin, the MC transports nutrient-rich waters northwards (Piola *et al.*, 2018). The collision between the MC with the warm-salty waters of the BC at approximately 38°S generates one of the most energetic regions of the world ocean: the Brazil Malvinas Confluence (BMC). After the collision, both currents deflect offshore and separate from the continental slope. A fraction of the BC flows northwards as the eastern limb of a recirculation cell feeding back into the BC (Valla *et al.*, 2018), while the other part of the BC follows the STF and overshoots southwards to about 45°S (the BC overshoot, **BCO**) before turning back to the north (Fig. 3). The MC retroflects cyclonically towards the south (the Malvinas Current Retroflection, **MCR**) flowing concurrently with the BCO. Thus, the region located between the SAF and the STF, which encompass the northern sector of the Patagonian margin, the Brazil Malvinas Confluence Zone (**BMCZ**), is characterized by intense near-surface velocities associated with fronts, eddies, meanders, and filaments. There, surface eddy kinetic energy (**EKE**) is among the greatest in the world ocean and mixes waters of different types and biogeochemical characteristics (Valla *et al.*, 2018).

The circulation in the studied region comprises four

water masses of Subantarctic origin: the light Surface Subantarctic Water (**SSAW**, upper 100 m), the Antarctic Intermediate Water (**AAIW**, between ~500–1000 m), the Circumpolar Deep Water (**CDW**, between ~1000–3500 m) and the Antarctic Bottom Water (**AABW**, below 3500 m) (Tsuchiya *et al.*, 1994; Arhan *et al.*, 1999, 2002). The upper layer of the Malvinas Current was defined by Artana *et al.* (2021) as a layer thicker than 800 m, the Malvinas Upper Water (MUW, $\theta > 2.5\,°C$ and $33.9 < S < 34.32$), which comprises the SSAW and the light upper AAIW (Fig. 4). The CDW is the deepest portion of the Antarctic Circumpolar Current (ACC; Orsi *et al.*, 1995) mainly formed in the Weddell Sea that circulates northwards along the western edge of the Argentine Basin. The southward flow of the North Atlantic Deep Water (**NADW**) splits the CDW into an upper CDW (**UCDW**) water mass and into a lower CDW (**LCDW**) water mass (Fig. 4). The UCDW is relatively fresh (S~34.58), cold ($2.65\,°C < \theta < 3.62\,°C$), and oxygen-depleted ($O_2$~188 µmol·kg-1), although its oxygen concentration and temperature increase due to mixing with the adjacent warmer and relatively more oxygenated water masses, the AAIW and the NADW (Valla *et al.*, 2018). Due to mixing with the underlying well-oxygenated AABW, the LCDW is, on average, more oxygenated than the UCDW ($\theta = 0.7\,°C$, O_2~215 µmol·kg^{-1}, S~34.72).

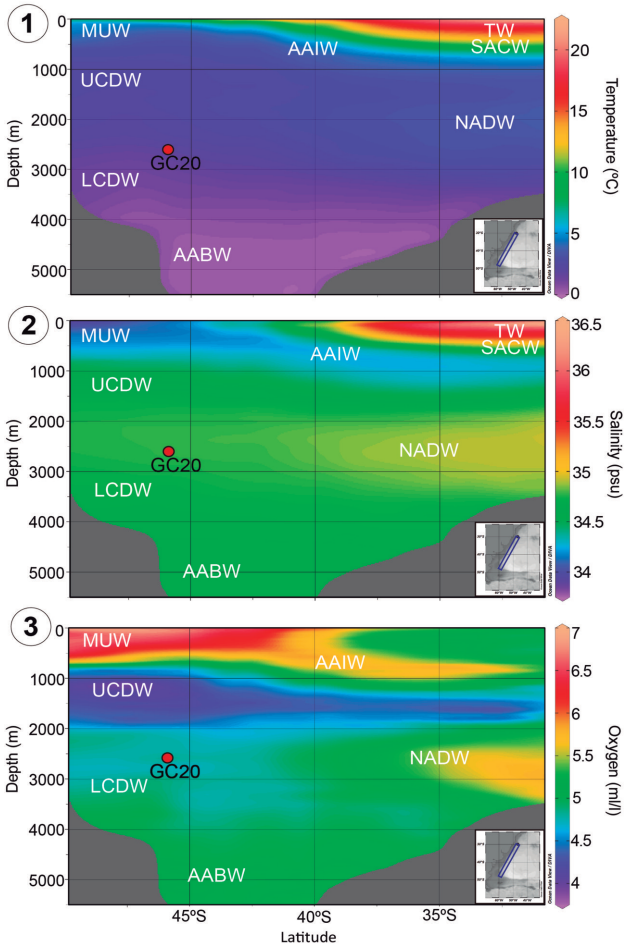

Figure 4. 1) Temperature, 2) salinity, and 3) dissolved oxygen sections of the western South Atlantic (Locarnini *et al.*, 2013; Zweng *et al.*, 2013; García *et al.*, 2014) showing the modern configuration of superficial, intermediate and deep-water masses. The dot represents the location of the studied core. **MUW**: Malvinas Upper Water; **TW**: Tropical Water; **SACW**: South Atlantic Central Water; AAIW: Antarctic Intermediate Water; **UCDW**: Upper Circumpolar Deep Water; **NADW**: North Atlantic Deep Water; **LCDW**: Lower Circumpolar; **AABW**: Antarctic Bottom Water.

According to satellite estimations, the western South Atlantic is one of the most productive areas of the world ocean (Lutz *et al.*, 2018). Excluding the inner shelf up to 50-60 m (Fig. 1), the primary productivity is highly variable in time and space over the Patagonian shelf with Chl-a concentrations of up to ~20 mg m^{-3} during spring and summer (García *et al.*, 2008; Lutz *et al.*, 2010). North of 46°S, blooms occur throughout the shelf during spring, whereas towards the summer, high satellite Chl-a concentrations are detected only south of 46°S. However, the shelfbreak continues to be productive during the entire warm season from between 38°S to the latitude of the Malvinas Islands, where a band of high satellite Chl-a can be detected along the entire shelfbreak. Whereas intense upwelling along the shelfbreak favors macro-nutrient availability (Carranza *et al.*, 2017), iron shelf transport probably contributes to maintaining the spring bloom (García *et al.*, 2008).

Local geological settings

Between 38°–55° S, the Patagonian continental Margin (**PCM**) is formed by a broad plateau of 350 km subject to the intense action of the SWW (Piola *et al.*, 2018). The shelfbreak, the transition between the shelf and the upper slope, occurs at depths of 110–165 m (Cavallotto *et al.*, 2011; Violante *et al.*, 2014), with a general trend of increasing depths towards the south (Parker *et al.*, 1996). The slope comprises the southern part of the giant Contourite Depositional System that extends through the entire Argentine continental margin (Hernández-Molina *et al.*, 2009). This contouritic system shows different morpho-sedimentary features, either erosional, depositional, and

mixed. In the PCM, four terraces of relative low gradient can be recognized: the Nágera (at ~500 m water depth), Perito Moreno (at ~1000 m), Piedra Buena (between 2100–3200 m), and Valentín Feilberg (between 3500–4000 m) (Hernández-Molina *et al.*, 2009; Violante *et al.*, 2017). The latter connects directly with the abyssal plain; thus, the continental rise is not distinguishable (Cavallotto *et al.*, 2011). Besides these conspicuous morphosedimentary features, the PCM hosts a vast canyon system (Ewing & Lonardi, 1971; Lastras *et al.*, 2011; Bozzano *et al.*, 2017), which comprises seven main canyons and more than 50 tributary canyons between 500 and 1800 m. These canyons cut the Nágera and Perito Moreno terraces and eventually indent the shelfbreak (Lastras *et al.*, 2011). To the east, the canyon system continues through the Piedra Buena Terrace and finally conveyed into a contouritic channel at the boundary between Piedra Buena and Valentín Feilberg terraces at water depths of ~3500 m (Hernández-Molina *et al.*, 2010; Isola *et al.*, 2021).

The core analyzed in this work was retrieved from the Piedra Buena Terrace (Fig.2), which is currently bathed by the LCDW (Figs. 3 and 4). The uppermost sedimentary record is composed of an alternation of mixed-contouritic terrigenous silty/sandy sediments with pelagic calcareous ooze (Isola *et al.*, 2021; Murdmaa *et al.*, 2018). The correlation of these sedimentary facies with seismic records suggests that the onset of this cyclic alternation could have started after the Mid–Pleistocene Transition (Isola *et al.*, 2021) and could be somehow associated with the quasi-100 ka glacial-interglacial cycle that characterizes Middle and Late Pleistocene. Although direct measurements of bottom-current velocity for the LCDW at the Patagonian margin have not yet beenreported, estimations of 7–17 cm s^{-1} have been inferred north of 43.5° (Gruetzner *et al.*, 2012). Other studies have shown that the overall intensity and vertical position of the LCDW in the western South Atlantic varied markedly across the last glacial cycle (Preu *et al.*, 2012; Roberts *et al.*, 2017; Warratz *et al.*, 2017, 2019).

MATERIALS AND METHODS

Sediment core AU_Geo02_GC20 (312.5 cm) was collected onboard R/V Austral (CONICET) during the YTEC-GTGM 2017 sampling program. The coring site is located at the Piedra Buena Terrace at 2589 m water depth at 45° 55.914′ S; 58° 30.126′ W. The site corresponds to the BMCZ as defined above. The basal sediment (312.5–213 cm) (Fig. 5) consists of olive-gray muddy sands with sand lenses at 268–248 cm and 228–213 cm. The overlying 31 cm (146–115 cm core depth) consists of gray and greenish-gray fine sands and gray and very dark olive-gray muddy sands and displays a general finning-up trend; the contacts with the overlaying and underlying strata are transitional. Between 115–42 cm, sediment is composed of white clayey foraminifer-bearing nannofossil ooze with small, very dark olive-gray sandy patches. The overlying 22 cm is composed of gray and dark olive gray medium and fine sands with isolated fine pebbles. The grain-size decreases near the top of this interval. The uppermost 16 cm of the core is composed of fine sand with abundant foraminifera and isolated dark pebbles and cobbles.

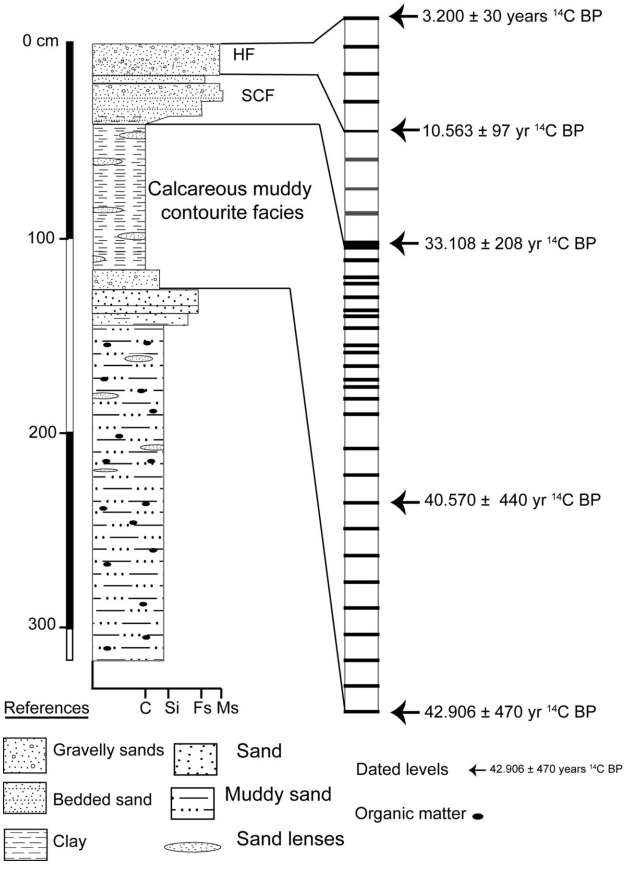

Figure 5. Schematic stratigraphic log of core AU_Geo02_GC20 with the facies described in this study. The column at the right of the log shows the position of the 35 samples analyzed and the AMS ^{14}C dating performed. **HF**: hemipelagic facies; **SCF**: sandy contourite facies.

In this paper, we focused our analyses on the upper 120 cm of the core, the interval that includes the white clayey foraminifera nannofossil ooze. The core was then continuously sub-sampled at 5-cm intervals between 120 and the top, although additional samples were taken at key levels. As a result, 35 subsamples were obtained.

Sediment chronology

The age model from the uppermost 120 cm of core AU_Geo02_GC20 is based on linear interpolation of 5 AMS ^{14}C datings (Tab. 1). Samples were analyzed at Beta Analytics and DirectAMS laboratories (United States). Dates were calibrated with the IntCal20 curve (Reimer *et al.*, 2020) and corrected taking into account the reservoir ages derived from Butzin *et al.* (2017). The age-depth model was developed using the code clam package (Blaauw, 2010) in R version 3.2.1 (R Core Team, 2018). All ages are given in calibrated thousands of years before present (**ka BP**). Accumulation rates (**AR**) were calculated as ka cm^{-1}, whereas linear sedimentation rates (**LSR**) were calculated between dated levels as cm ka^{-1}.

Foraminifera analyses

Samples for foraminiferal analyses were weighed and wet-sieved using a 63 µm mesh sieve to obtain the sand-sized fraction. Benthic and planktonic specimens were individually picked. Samples with less than 300 individuals were not taken into account for statistical analyses. Samples with less than 50 benthic individuals were not taken into account for reconstructions because we consider that results from a smaller sample size can be questionable.

For the count of planktonic foraminifera, the residue was dried, weighed again, and then sieved using a 150 µm mesh sieve. After sieving, samples were divided using a microsplitter, and at least 300 individuals were picked for each sample for statistical purposes. The specimens were identified using the species concepts of Kennett and Srinivasan (1983) and Hemleben *et al.* (1989). The taxonomic nomenclature was harmonized following the criteria established by Brummer and Kucera (2022). Given that the original taxonomy facilitates the grouping of some species and enables the harmonization of possible taxonomic differences between assemblages, these groups were preserved as multi-species categories. We applied this criterion to the "*cultrata ex-menardiforms complex*" group, which includes the species *Globorotalia cultrata* (d'Orbigny, 1839), *Globorotalia tumida* (Brady, 1877) and *Globorotalia ungulata* (Bermúdez, 1961), and to the "*Globigerinoides ruber* total" group, which includes the white and pink morphotypes of *Globigerinoides ruber* (d'Orbigny, 1839). As the ratio between neogloboquadrinids *Neogloboquadrina pachyderma* (Ehrenberg, 1861) and *Neogloboquadrina incompta* (Cifelli, 1961) is controlled by water temperature, with the former dominating in cold waters with mean annual SST of 8°C (Eynaud, 2005) and *N. pachyderma* dominating the ecosystem in polar regions starting from 50° S (Lombard *et al.*, 2011), we calculate the *N. incompta-pachyderma* ratio as the relative abundance of *N. incompta* over the sum of *N. pachyderma* and *N. incompta* for SST qualitative estimation. As both species show biasses in coiling preferences, we follow Darling *et al.* (2006) for specific identification. In the case of benthic foraminifera, all specimens within the

TABLE 1. Radiocarbon ages used to produce the age model of sediment core AU_Geo02_GC20

Depth (cm)	Species	Age dated (^{14}C year BP)	Lab error (years)	Calibrated age (cal. year BP)	Laboratory
0	***G. inflata***	3200	30	2538	Beta Analytic
20	***G. inflata***	10563	90	10927	DirectAMS
45	***G. inflata***	33108	208	36133	DirectAMS
80	***G. inflata***	40570	440	42534	Beta Analytic
120	***G. inflata***	42906	470	44027	DirectAMS

sample > 63µm were picked and counted. At the generic level, the taxonomic identification follows Loeblich and Tappan (1988), whereas relevant literature for the studied area was used to identify species (*e.g.*, Boltovskoy *et al.*, 1980 and cites therein). The relative abundances (%) of each benthic/planktonic species in the whole benthic/planktonic assemblage and the total number of benthic and planktonic individuals per gram of dry sediment (the benthic foraminifera number - **BFN** and the planktonic foraminifera number - **PFN**) were calculated for each sample.

Different foraminifera-based indices frequently used to estimate primary productivity and flux of particulate organic matter to the bottom floor were estimated. These include: **a)** the ratio between planktonic and benthic foraminifera (P/P + B ratio) calculated as the PFN over the sum of the PFN and the BFN; this ratio usually depends on the supply of particulate organic matter (**POC**) from the photic zone to the seafloor, the so-called exported production (Berger and Diester-Haas, 1988); **b)** the eutrophic productivity index (**FPI**, Bostock *et al.*, 2019), calculated as the sum of the relative contribution (%) of *Globigerina bulloides* (d'Orbigny, 1826), *Globigerinita glutinata* (Egger, 1893), and *Turborotalita quinqueloba* (Natland, 1938); this index was calculated since these species dominate seafloor assemblages in regions of the South Hemisphere with high sea surface primary productivity (Crundwell *et al.*, 2008); **c)** the shell flux of the planktonic species *G. bulloides* (number of shells cm^{-2} ka^{-1}), calculated as the number of *G. bulloides* shells in >150 µm fraction per gram of dry sediment multiplied by the LSR and the dry bulk density (**DBD -**g cm^{-3} -, the ratio between the mass of dry sediment and the volume of the sample); values higher than 400 shells cm^{-2} ka^{-1} are considered indicative of very high primary productivity such as those prevailing in upwelling regions (Lombard *et al.*, 2011); **d)** the benthic foraminifera accumulation rate (**BFAR**), a proxy for export productivity (Herguera, 1992), was also calculated according to Herguera and Berger (1991); for the BFAR calculation, the BFN was multiplied by the LSR and the DBD; therefore, the BFAR is expressed as the number of benthic individuals cm^{-2} ka^{-1}; finally, **e)** the relative abundance of selected benthic foraminifers *Uvigerina peregrina* (Cushman, 1923), *Oridorsalis umbonatus* (Reuss, 1851) and *Cibicidoides wuellerstorfi* (Schwager, 1866) were used as proxies of organic carbon flux rates and/or organic matter quality due to their particular ecological demands: *U. peregrina* is a shallow infaunal species common at bathyal depths and in areas of high surface productivity or lateral advection of refractory organic matter; *O. umbonatus*, a cosmopolitan taxon of lower bathyal and abyssal depths, is a shallow infaunal species (Brown *et al.*, 2011) typical of well-oxygenated deep waters and hence moderate to low particulate organic carbon fluxes (Gupta *et al.*, 2008); finally, the epifaunal species *C. wuellerstorfi*, a cosmopolitan species thriving in all deep-sea basins, also indicates low organic-matter fluxes to the sea bottom (Gooday, 2003). Additionally, total carbon (**TC**) was calculated by Loss-on-ignition (**LOI**) according to Heiri *et al.* (2001) at Laboratorio de Sondeos de Ambientes Continentales y Marinos (SACMa, IDEAN) facilities. Considering the treatment of the samples with hydrogen peroxide did not produce a visible reaction nor sediment color lightening, TC is considered nearly equal to the sum of the inorganic carbon species. Sand content (%), TC, BFN, and PFN were used to define sedimentary facies.

Sea-surface temperature and nutrient and quantitative estimations

The sea surface temperature was estimated by applying the modern calibration function proposed by García Chapori and Laprida (2021). This transfer function is based on a calibration dataset specifically developed for the western South Atlantic that includes samples from between 0°–60°S and 0°–70°W and covers the whole environmental gradient of the South Atlantic. It shows the most precise reconstructions for the annual mixed layer temperature (**SST_{50}**) at 50 m water depth (r^2_{jack}=0.94; RMSEP=1.87). Additionally, a new South Atlantic planktonic foraminifera-based transfer function for reconstructing primary productivity-related parameters from the South Atlantic was developed by Albarracín (2021). The dataset includes core-top samples selected from Siccha and Kucera (2017), García Chapori and Kucera (2019), and core-top samples collected from the continental margin of Argentine and Uruguay 36°S–39°S (Kasten *et al.*, 2019). Environmental variables associated with productivity were selected: phosphate, nitrate, Chl-a, iron (Fe), particulate organic carbon (POC), and the absorption coefficient of phytoplankton at 443 nm (aph443). Seasonal values of phosphate, nitrate, Fe, Chl-a, and POC at each site were

considered as these values mark the spatial distribution of seasonal productivity processes of the Patagonian shelfbreak upwelling (Valla & Piola, 2015). The significance of each environmental variable was tested following Juggins (2013). To establish the transfer function, different models (Weighted Averaging, (**WA**), Weighted Averaging-Partial Least Squares (**WA–PLS**), and Maximum Likelihood (**ML**)) were tested, and the best model was identified according to Birks (1995). Outliers were identified according to Birks *et al.* (1990) and Zuur *et al.* (2007) and removed from the analysis. Further details regarding the transfer function development will be published elsewhere.

RESULTS

The upper 120 cm of the sediment core AU_Geo02_GC20 spans approximately the last 44 ka (Fig. 6) and hence represents sediments deposited from the last part of the MIS 3 to the Late Holocene. Still, although erosional surfaces were not identified during the visual examination of the core, the abrupt lithological change between 42–38 cm (Fig. 5) could imply that the age model potentially incorporates a short hiatus in this interval. Thus, calibrated ages in the interval 33.1-29 ka BP must be taken with caution. The uppermost 38 cm spans MIS 2 (29–14 ka BP) and MIS 1 (the last 14 ka BP). According to the age model, the average sedimentation rate is 11 cm ka^{-1}. The highest LSR (Fig. 6) occurred in a very short interval between 44 and 42 ka BP (26.7 cm ka^{-1}), and the lowest LSR (0.99 cm ka^{-1}) occurred during the MIS 2.

The TC along the core is highly variable (Fig. 7), ranging from 6.62% to 47.12%, with maximum values occurring between 39.8 and 37 ka BP (average: 44.3%) and minima occurring between 26.0 and 16.0 ka BP during the MIS 2 (average: 7.76%). The DBD (Fig. 7) oscillates between 0.56 and 1.24 g cm^{-3} with maximum values between 33.6 and 10.9 ka BP (>1 g cm^{-3}) and minima between 42.5 and 37 ka BP (average 0.63 g cm^{-3}). The overall trend of sand content (Fig. 7) mirrors the DBD and oscillates between 3.0 and 54.9%, showing a quasi-monotonous increase since 36.7 ka BP showing maximum values (>30%) between 33.6 ka BP and 10.9 ka BP, with a conspicuous peak of 55% at 21 ka BP. As expected, DBD is negative and significantly correlated with TC (r^2= -0.94; p<< 0.01) and positive and significantly correlated with sand content (r^2=0.89; p<< 0.01).

Four samples were omitted from micropaleontological analyses: the samples between 31–11 ka BP were considered barren of foraminifera (see Materials and Methods section). According to the age model, these samples correspond to the interval 26.0–16.0 ka BP (MIS 2), including the Late Glacial Maximum (21 ka BP). As mentioned above, these samples showed the lowest values of TC (8.6–6.6%) and the highest contribution of sands (39.5–54.9%) (Fig. 7). Additionally, the sample taken at 85 cm showed deviant values in the parameters based on foraminiferal assemblages that do not fit the general trend over time. The benthic and planktonic assemblages recovered from this level are considered not representative of the paleocommunities due to syn- and/or post-depositional processes. The foraminiferal-based parameters calculated from this level are considered outliers and omitted from the discussion.

Besides these samples, the PFN (Fig. 7) varies substantially along the core, ranging between 327 and 6981 ind. g^{-1}. High PFN values (>2000 ind. g^{-1}) are observed between 44.0–42.9 ka BP. After that, values are somewhat lower and rather irregular, with two conspicuous minima between 33.6-32.1 ka BP and 6.7-4.6 ka BP. A total of 21 species were identified, of which only nine showed total abundances >2% in at least two samples (Tab. 2). The overall fauna is dominated by *G. bulloides* (mean 35.1%), followed by *Neogloboquadrina incompta* (mean 23.2%), *Neogloboquadrina*

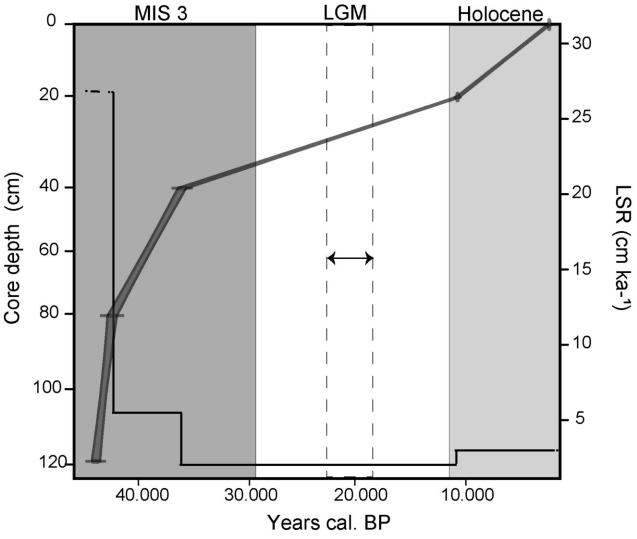

Figure 6. Age model and linear sedimentation rate (LSR) of the core AU_Geo02_GC20. The MIS 3 is represented by a dark gray vertical shade, the LGM is represented by a dashed square, and the Holocene is represented by a light grey shade.

pachyderma (mean 18.5%), *Globoconella inflata* (d'Orbigny, 1839) (mean 9.1%), *Globigerinita glutinata* (mean 3.5%), *Globorotalia hirsuta* (d'Orbigny, 1839) (mean 3.2%), T*urborotalita quinqueloba* (mean 2.4%), *Neogloboquadrina dutertrei* (d'Orbigny, 1839) (mean 1.1%) and *Globorotalia truncatulinoides* (d'Orbigny, 1839) (mean 0.7%). The relative abundance of *G. bulloides* (Fig. 7) ranged from 17.3 to 48.7% along the core. The higher values occurred during MIS 3 (44–31.1 ka BP) when abundance ranged from ~20–48%, and during the mid–Holocene, when the abundance ranged from ~39%–44%. During MIS 3, abundances were usually high (>40%) between 42.7–38.1 ka BP (mean: ~43%) and tend to decrease between 42.5–31.1 ka BP (mean: ~33%), while during the Holocene, although values are still high (>17%), mean abundance is slightly lower (mean: 31%). The relative abundance of *N. pachyderma* (Fig. 7) displays the opposite behavior during MIS 3, ranging from 9.5 to 39.3% between 44-42.7 ka BP and decreasing after 42.5 ka BP (2.7–33.8%). During the Holocene, *N. pachyderma* shows values between 18–36.2%. Between 42.5–31.1 ka BP, the relative abundance of *N. incompta* (Fig. 7) ranges from 13.5–30.5% and increases to 36%–22.4% (mean of 26.1%) between 42.5–31.1 ka BP. During the Holocene, this species shows its lower abundance oscillating between 2.7–19%, the lowermost value registered at 8.8 ka BP in the early Holocene. The abundance of *G. inflata* remains nearly constant during MIS 3, with an average of 8.1%, with the lowest values at the base of the core. The highest values occurred during the Holocene, ranging between 14–18%, interrupted by a minimum of 7% at 4.6 ka BP. The abundances of *G. glutinata* and *T. quinqueloba* were low and nearly constant along the core, with average values of 3.7% and 3.5%, respectively. *G. hirsuta* is found exclusively in samples from MIS 3; its abundance attains a maximum between 42.5–37 ka BP, with an average of 4.6%, whereas the stratigraphic distribution of *G. truncatulinoides* and *N. dutertrei* are restricted to isolated levels along the core, showing abundances lower than 3%.

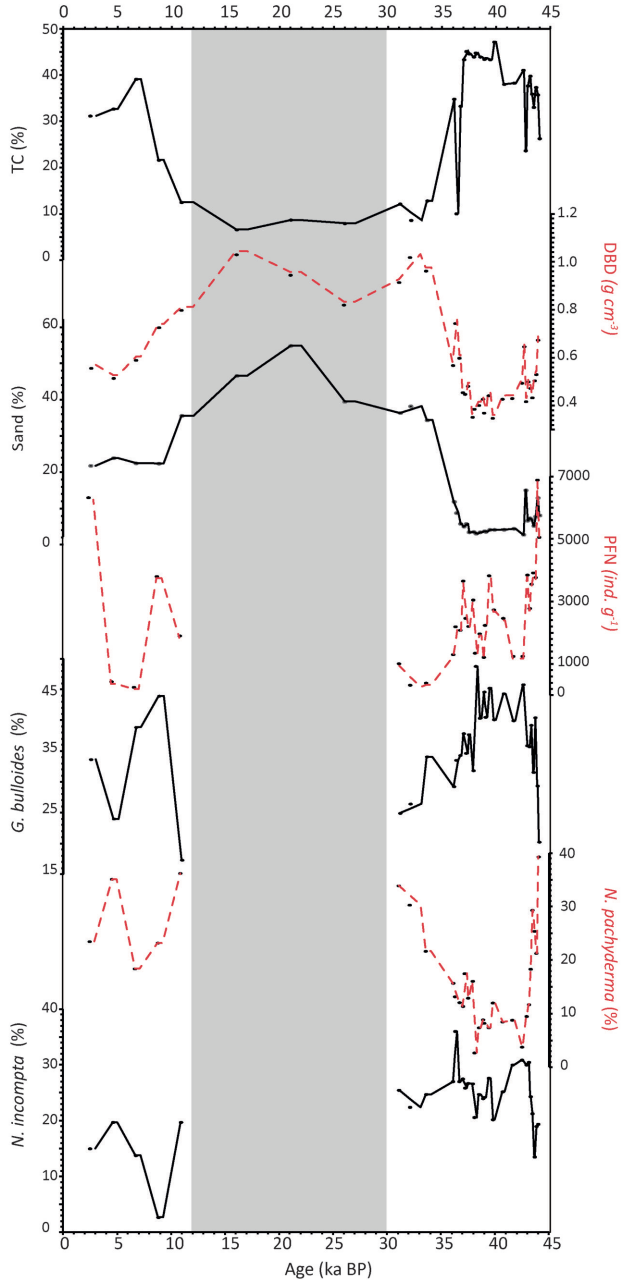

Figure 7. Proxy records from core AU_Geo02_GC20. **TC**: Total carbon (%). **DBD**: dry bulk density. **PFN:** planktonic foraminiferal number (individuals per gram). The grey bar represents levels barren of foraminifera or excluded from the analyses. Two-point moving average smoothing has been applied to all parameters.

The FPI shows moderate fluctuations throughout the core (Fig. 8), oscillating between 23.9 and 52%. The highest FPI values (>45%) are found between 42.5–38.1 ka BP. Since 38.1 ka BP, the FPI shows a clear decreasing trend towards the end of MIS 3. FPI reaches the lowest value during the onset of the Holocene (24%) and increases markedly during the mid-Holocene (>45%). The FPI closely mirrors the relative abundance of *G. bulloides* (r^2= 0.97; p<< 0.01). In contrast, the flux of *G. bulloides* (Fig. 8) varies substantially through the core, with most values ranging between 100–500 ind. cm^{-2} ka^{-1}. Higher values were recorded during MIS 3, at 44.0, 43.5–43.2 ka, and between

TABLE 2. Species of planktonic foraminifera found in the core AU_Geo02_GC20 and their employment in the developed transfer function.

Included	Excluded
Globorotalia hirsuta	*Globorotalia scitula*
Globorotalia truncatulinoides	*Berggrenia pumilio*
Globoconella inflata	*Globigerina falconensis*
Neogloboquadrina dutertrei	*Globigerinoides ruber (total)*
Neogloboquadrina incompta	*Trilobatus sacculifer*
Neogloboquadrina pachyderma	*Globigerinella siphonifera*
Globigerina bulloides	*Turborotalita humilis*
Turborotalita quinqueloba	*Globoturborotalita rubescens*
Globigerinita glutinata	*Globigerinita uvula*
	Tenuitella iota
	Globigerina bermudezi
	Globigerinoides parkerae

36.1–32.1 ka BP, with a very prominent peak at 43.2 ka with ca. 3000 ind. cm^{-2} ka^{-1}. The ratio between *N. incompta* and *N. pachyderma* (Fig. 8) is higher than 0.5 between 43.2–36.3 ka BP, attaining higher values between 42.5–38.1 ka BP. Since 36.3 ka BP, values decrease abruptly and monotonically, achieving ca. 0.4 towards the end of the MIS 3. During the early Holocene, the ratio *N. incompta* and *N. pachyderma* attains its lowest value (0.1), increasing thereafter during the mid and late Holocene, oscillating around 0.4.

The BFN (Fig. 8) shows surprisingly low values, ranging between 6–170 ind. g^{-1}. During MIS 3, the BFN tends to be extremely low, with most values lower than 15 ind. g^{-1}. However, the values are somewhat higher between 43.8–42.5 ka BP and 36.1–33.6 ka BP. The highest BFN values (>150 ind. g^{-1}) were found at mid and late–Holocene samples. The BFAR (Fig. 8) ranges between 8.6–934 ind. cm^{-2} ka^{-1}, showing higher values between 44.0–42.5 ka (average: 560 ind. cm^{-2} ka^{-1}) and displaying a secondary peak during the Holocene, with an average of 163 ind. cm^{-2} ka^{-1}. The P/P+B ratio is > 0.95 for most samples, except for the mid–Holocene, where the P/P+B ratio varied between 0.63 and 0.73 (results not shown).

The relative contribution of the shallow infaunal species *U. peregrina* (Fig. 8) and *O. umbonatus* (Fig. 8) vary substantially along the core. Relative abundance of *U. peregrina* oscillates between 2.1% and 69.6% (average: 19.9%). Higher values were found between 38.5–36.3 ka BP (>20% and up to 45%), and increasing markedly during the Holocene (48–70%),

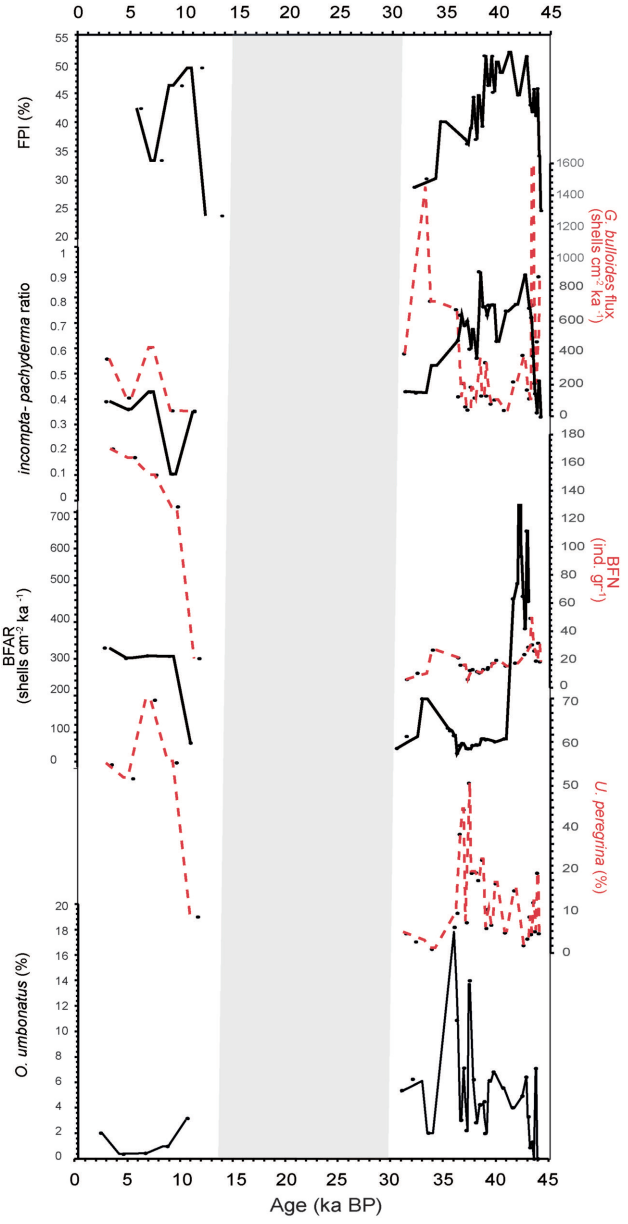

Figure 8. Proxy records from core AU_Geo02_GC20. **FPI**: eutrophic productivity index (%). **BFN**: benthic foraminifera number (individuals per gram). **BFAR**: benthic foraminifera accumulation rate. The grey bar represents levels barren of foraminifera or excluded from the analyses. Two-point moving average smoothing has been applied to all parameters.

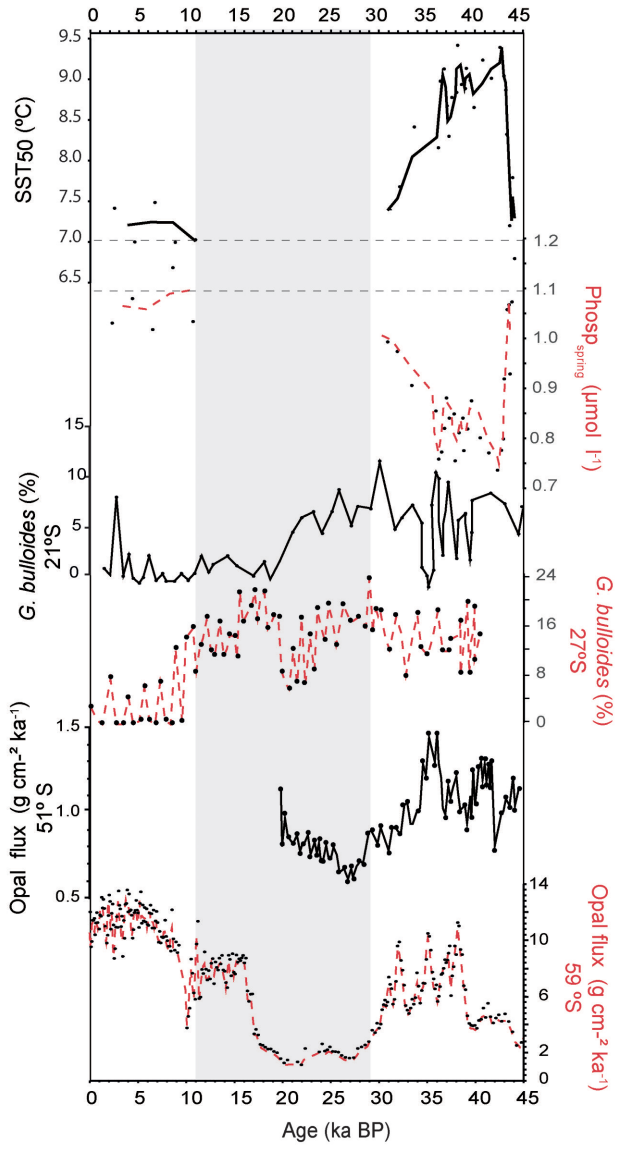

Figure 9. Proxy records from core AU_Geo02_GC20 and comparison with western South Atlantic and Southern Ocean records. **SST_{50}**: subsurface temperature at 50 m depth (°C); the triangle in the axis indicates mean annual modern values. **$Phosps_{pring}$**: spring phosphate (µmol l^{-1}); the triangle in the axis indicates mean spring modern values. In both cases, two-point moving average smoothing has been applied. The relative abundance of *Globigerina bulloides* (%) at 21°S corresponds to the sediment core GL75 (21° 08' 32.00" S; 40° 01' 22.08" W; water depth of 1421 m), subtropical brazilian margin (modified from Portilho Ramos *et al.*, 2015). The relative abundance of *Globigerina bulloides* (%) at 27°S corresponds to the sediment core GeoB2107-3 (27° 10' S; 46° 27' W, 1048 m water depth), in the South Brazilian Bight (modified from Pereira *et al.*, 2018). The Opal flux at 51°S corresponds to the core TN057-14PC (51° 59' S; 4° 31' E, 3648 m water depth), a proxy for the CDW upwelling in the Southern Ocean (modified from Anderson *et al.*, 2009). Opal flux at 59°S corresponds to the sediment core MD07-3134 (59° 25' S; 41° 28' W, 3663 m water depth), a proxy for the CDW upwelling in the Southern Ocean (modified from Sprenk *et al.*, 2013). The grey bar represents the levels barren of foraminifera.

when it becomes the dominant species. In all the samples, the relative contribution of *O. umbonatus* (average: 4.5%) is lower than those of *U. peregrina.* The relative abundance of *O. umbonatus* tends to be higher during MIS 3 between 37.5 ka BP and 36.1 ka BP (average: 9.2%), attaining its higher value (18% 9 at 36.1 ka BP. Holocene values are usually lower than 2% (Fig. 8). Finally, although *C. wuellestorfi* is frequently rare and relative abundances are usually lower than 2%, values are highly variable during MIS 3, reaching higher values (5–9%) between 39–35 ka BP (results not shown).

Sea surface and primary productivity-related parameters reconstructions

The reconstructed downcore variations of the annual mean SST_{50} oscillates between 9.4°C and 6.8°C (Fig. 9), with both the highest and the lowest values recorded during MIS 3. However, when reconstructions are analyzed in deep, most annual mean SST_{50} reconstructions between 43-36.3 ka BP represent significant positive anomalies (>RMSEP) compared with the modern reference value (6.9°C, Locarnini *et al.*, 2013). SST values increase from 6.8°C at 44.0 ka to 8.3°C at 43.2 ka BP, and thereafter increase rapidly to attain a maximum of 9.4°C at 38.1 ka BP. The reconstructed SST_{50} between 43.2 and 33.6 ka BP oscillates between 9.4°C to 8.2°C, implying a mean positive anomaly of ca. 2.0°C. During the Holocene, reconstructed SST_{50} values fluctuate between 7.0 and 7.5°C within the reconstruction error.

The transfer function applied for primary productivity-related parameter reconstruction showed that spring phosphate (**$phos_{spring}$**) can be reconstructed with a high statistical significance. The reconstructed $phos_{spring}$ values range between 0.74 and 1.14 µmol l^{-1} (Fig. 9). Reconstructed values decrease from 1.07 to 0.74 between 44–42.5 ka BP, and after that, $phos_{spring}$ slightly increases showing rapid fluctuations between 41.6 and 36.3 ka BP (mean 0.81 µmol/l). Subsequently, $phos_{spring}$ increases uniformly between 36.1 and 31.1 ka BP when the values range between 0.85 and 0.99 µmol/l. During the Holocene, $phos_{spring}$ reach higher values, ranging between 1.02 and 1.14 µmol/l, which are close to modern values. The mean annual SST_{50} is nega-tively correlated with spring phosphate (r^2= -0.97, p<< 0.01).

DISCUSSION

Sedimentary facies

The depositional history of the PCM has been strongly influenced by the northward-flowing, southern-sourced deep water masses since the opening of the Drake Passage in the Miocene (Hernández-Molina *et al.*, 2009, 2010). As such, a wide range of different facies that fall within contourites' spectrum was recognized in deep-water deposits of the PCM, including low energy-related facies (Bozzano *et al.*, 2011). Based on sand content, TC, BFN, and PFN, three distinctive contourite facies were recognized in the section analyzed of the core AU_ Geo02_ GC_20: the calcareous muddy contourite facies, the sandy contourite facies, and the hemipelagic facies (Fig. 5).

The calcareous muddy contourite facies (120–42.5 cm) was deposited between 44–33.6 ka BP. The composition is typically pelagic and includes mainly calcareous nannoplankton and planktonic foraminifera. Benthic foraminifera, radiolaria, and diatoms are subordinated. The contribution of the sand fraction is <15%, and TC is usually higher than 35% (Fig. 7). The mean grain size is silty clay to clayey silt with a distinct sand-sized fraction represented by biogenic particles, *e.g.*, planktonic and benthic foraminifera. PFN is higher than 1200 ind. gr^{-1} (Fig. 7), whereas BFN oscillates between 50–6 ind. g^{-1} (Fig. 8). As the preservation of both planktonic and benthic foraminifera is very good, the downcurrent transport of the sand-sized biogenic material as bed load is discarded and thus, fossil assemblages can be considered as representatives of the paleobiocoenoses.

A coarsening-up sandy silt layer with horizontal lamination and gradational basal contact represents the onset of the deposition of the sandy contourite facies (42.5–20 cm). It is marked by the abrupt increase in sand content (>30%) and the abrupt decrease in TC (<12%), both parameters reaching the lowest values of the entire record in this facies (Fig. 7). The sandy contourite facies spans the uppermost MIS 3 and the whole MIS 2, including the Last Glacial Maximum (Fig. 6). The PFN decreased dramatically oscillating between 325–1000 ind. gr^{-1} and the BFN never exceed 27 ind. gr^{-1} (Figs. 7 and 8). The levels between 35 and 25 cm, assigned to the MIS 2, are barren of foraminifera. The abrupt increase in TC (between 12–39%) and the abrupt decrease in sand content (between 22–24%) since the early Holocene (10.9 ka BP; Fig. 7) mark the onset of the deposition of hemipelagic facies, where the BFN (Fig. 8) increases abruptly, although the PFN (Fig. 7) shows abrupt shifts and does not show a definite pattern. The coarse-grained material (mainly pebbles and cobbles) presents in the sandy contourite facies and the hemipelagic facies suggests rafting processes in the Patagonian margin during MIS 2 and the onset of the MIS 1, similar to those described from the Mar del Plata Canyon area (Bozzano *et al.*, 2020).

The Piedra Buena Terrace is under the influence of the LCDW, a very energetic water mass, especially during glacial periods (Duplessy *et al.*, 1988; Mulitza *et al.*, 2013; Preu *et al.*, 2013). Thus, the presence of fine-grained contourite facies during the Last Glacial could seem intriguing considering the erosive power of the Malvinas Current (Wilckens *et al.*, 2021). A similar sequence during MIS 3 has been described by Isola *et al.* (2021) from the nearby core AU_Geo02_GC21 (46° S, 58° W, 2379 m water depth), demonstrating that these deposits have a regional expression. According to Isola *et al.* (2021), during the relatively high sea-level events of the MIS 3, the LCDW/AABW interphase would have been located at its modern position (Fig. 2.2). The slowing down of the bottom circulation due to the weakening of the Atlantic Meridional Overturning Circulation (AMOC) during MIS 3 (Menviel *et al.*, 2015) in conjunction with enhanced primary productivity in the PCM would have favored the settling down of pelagic particles over the terrace. Records from the western subtropical South Atlantic covering the last glacial cycle allow inferring a reduction in the AMOC strength during the Heinrich stadials of MIS 3 (Portilho-Ramos *et al.*, 2015; Pereira *et al.*, 2018). The shoaling and the lower flux of North Atlantic Deep Water (NADW) into the Southern Ocean under cooler, glacial conditions (Menviel *et al.*, 2015; Curry & Oppo, 2005) could have expanded the accommodation space for the AABW, shifting down the AABW-LCDW interphase. A glacial downshift of the intermediate-deep water masses interphases has also been proposed by Steinmann *et al.* (2020). After that, the resumption of the AMOC and the strengthening of the southern-source circulation, especially during MIS 2 (Mulitza *et al.*, 2013; Preu *et al.*, 2013), could have given place to the sandy-silty contourite facies deposition by the reinvigorated deep circulation. The very low abundance of foraminifera (Figs. 7 and 8) and the sharp decrease in the TC (Fig. 7) in this facies suggest that the interphase

between the LCDW and the corrosive AABW was shallower during MIS 2. Sea-floor topography (*e.g.*, morphological depressions and undulations and the submarine canyons) of the Piedra Buena Terrace would have favored the burying and the preservation of the calcareous muddy contourite facies, allowing fast burial and avoiding its erosion by the more vigorous bottom currents during the MIS 2. Present-day deep circulation and depositional type at the Piedra Buena Terrace began at the base of the MIS 1. Increased carbonate content and PFN since 11 ka BP (Fig. 7) indicates that the LCDW-AABW interface shifted downslope during the present interglacial (Warratz *et al.*, 2017), favoring carbonate preservation.

Potentials and constraints of the AU_Geo02_GC20 record

The core analyzed contains Late Pleistocene–Holocene paleoceanographic records with very high LSR during a short period during the last part of MIS 3 (Fig. 6), allowing the development of a high-resolution paleoceanographic reconstruction based on multiproxy analyses. Due to the geographical position of the PCM, the dominant action of bottom currents on the sedimentary record at the coring site is ascertained. However, the fine-grained pelagic facies described here could not have been deposited under the direct influence of strong bottom currents. The deposition of the calcareous muddy contourite facies implies that the vertical settling of pelagic particles through the water column between 44–33.6 ka BP dominated over the along-slope transport of the southern-source bottom currents. Although these currents could have affected the geometry of the sedimentary bodies after deposition, this pelagic facies was (at least partially) preserved and carried micro-fossils that contain a unique primary source of information about the paleoceanographic conditions of the PCM during the last part of MIS 3.

The excellent preservation of the calcareous fauna and the P/P+B ratio allow discarding significant dissolution and/or reworking processes that could affect the composition of the foraminiferal assemblages for most of the MIS 3. Although beyond the scope of this paper, similar considerations can be made for samples deposited during MIS 1. Only one isolated sample at 85 cm (42.7 ka BP) shows anomalous values in all assemblages-based parameters (*e.g.*, *N. incompta*/ *N. pachyderma* ratio, FPI, $phos_{spring}$, SST_{50}), in coincidence with random values of sand and TC. This seems to indicate that synsedimentary and/or biostratinomic processes affected the composition of both benthic and planktonic assemblages.

Conversely, an intense episode of carbonate dissolution was identified in sediments assigned to MIS 2, in coincidence with the sandy-silty contourite facies deposition. Episodes of carbonate dissolution in the western South Atlantic were frequent during the Neogene (Bertels & Núñez, 1989) and especially during the Last Glacial (Cusminsky, 1991, 1992). Unfortunately, the virtual absence of foraminifera in this facies hindered the reconstruction of surface parameters and paleoceanographic conditions based on foraminiferal indexes. Additionally, the low temporal resolution (ca. 2 ka) due to the low LSR during holocene times (Fig. 6) precludes the use of foraminiferal assemblages for any reliable paleoceanographic interpretation.

Even when taphonomic (neither biostratinomic nor fossildiagenetic) processes did not alter most of the foraminiferal assemblages in samples corresponding to MIS 3, several inconsistencies arise when interpreting some of the proxies. Due to the low values of the BFN, the P/P+B ratio is considerably constant and closely follows the PFN (r^2= 0.89; p<< 0.01), which is, on average, much higher than 159 times the BFN. Besides, the PFN attains extremely high values (5000-7000 ind. g^{-1}), suggesting extremely high productivity between 44–43.7 ka BP, while other productivity proxies, such as the *G. bulloides* flux , do not. Neither the values of the BFN nor the structure of the benthic assemblages nor the BFAR allow for inferring exceptionally high productivity during MIS 3 (Fig. 8). The BFAR strongly correlates with LSR during MIS 3 (r^2=0.91; p<< 0.01) and thus, it is not driven by productivity but by drastic changes in LSR (Fig. 6).

Apart from the impact of the LSR on the BFAR, the lack of relationship between the high phytoplankton abundance and productivity reconstructions based on planktonic foraminifera with the benthic productivity proxies seems to indicate a benthopelagic decoupling during MIS 3, when calcareous nannoplankton dominated the primary productivity. In well-stratified ecosystems, it is common for nannoplankton to dominate over diatoms as primary

producers. When this dominance is significant, it substantially reduces the efficiency of the biological pump (Cermeño *et al.*, 2008), decoupling pelagic and benthic communities' by reducing the exported production. Larger phytoplankton cells with siliceous skeletons, such as diatoms have a greater chance of resulting in greater export efficiency than smaller cells with calcareous skeletons, whose sinking velocities are extremely low (Mouw *et al.*, 2016; Cai *et al.*, 2002). Our results indicate that during the deposition of the calcareous muddy contourite facies, other factors, such as bottom currents controlling the sedimentary dynamics or the grain size of bottom sediments, could have been more important than food availability to structure the benthic assemblages. Thus, in this particular case, the signal of the benthic foram-based proxies (BFN, BFAR, and the P/P+B ratio) do not reflect the high primary productivity the planktonic foraminifera do.

Paleoceanographic reconstruction during MIS 3

Our results show that the phytoplanktonic as well as foraminifera communities' structure of the North PCM has been subject to significant changes in the last 44.000 years. The planktonic-based productivity proxies (Figs. 7 and 8) show enhanced primary productivity between 44-33.6 ka BP encompassing a "hyperproductive" period between 42.5–38.1 ka BP similar to very productive areas of the world oceans, followed by a constant decrease towards the end of the MIS 3. Matching with this multi-millennial hyperproductive period, positive anomalies of SST_{50} (Fig. 9) and lower-than-present $phos_{spring}$ values prevailed (Fig. 9). A relatively short second pulse of enhanced productivity during the Middle Holocene did not show the SSTs nor phosphate anomalies of the MIS 3, but the low temporal resolution of the record during the Holocene does not allow the formulation of a reliable hypothesis concerning the primary productivity patterns. Unfortunately, barren levels corresponding to MIS 2 exclude any interpretation of primary productivity during full glacial times at the slope of the north PCM.

The surface and subsurface temperature of the water column is one of the most important factors controlling the planktonic foraminifera distribution worldwide (Morey *et al.*, 2005). However, the fact that $phos_{spring}$ is a significant explicative variable of the composition of the assemblages in the South Atlantic confirms that other parameters than the SST play important roles in explaining the planktonic species' distribution as previous works proposed (*e.g.*, Schiebel *et al.*, 2001; Lessa *et al.*, 2019). Since foraminifers are heterotrophic organisms, the $phos_{spring}$ could explain the structure of the communities through its influence on primary productivity. Patagonian waters have an N:P ratio that far exceeds the Redfield ratio (N>>P) (García *et al.*, 2008). The marked decrease in the concentration of $phos_{spring}$ (Fig. 9) in coincidence with high contributions of *G. bulloides* (Fig. 7.5) and FPI index values (Fig. 8) indicate an intensive use of this macronutrient during the hyperproductivity phase of MIS 3, suggesting that this macronutrient was a limiting factor of the planktonic foraminifera' communities. Notably, these events of enhanced primary productivity have taken place far from the shelfbreak front where the shelfbreak upwelling nowadays boosts primary productivity. Instead, the site AU_Geo02_GC20 is located in the BMCZ at the westernmost limit of the South Subtropical Convergence (**SSTC**) province defined by Longhurst (2006) (Fig. 10), an oceanic area with a high mean satellite-derived Chl-a concentrations and south of the BMC. Changes in the MC's mean intensity and volume transport and the stability of the BMC frontal system could have also shifted the SSTs and primary productivity patterns at the coring site.

The characteristics of the BMCZ depend on the intensity of the impinging currents. Several studies have identified the existence of volume transport anomalies of both the MC and the BC at the PCM. Artana *et al.* (2018, 2021) analyzed the variability of the MC transport south of 41°S. They reported recurrent blocking events at 48.5°S, during which the surface transport of the MC was reduced to less than half its long-term mean, most of them during summer and spring. Moreover, volume transport anomalies of the MC determine the position of the SAF over the patagonian slope (Artana *et al.*, 2016). During MC transport maxima, the SAF extends north of 40°S and is pushed eastward of its mean location; in contrast, during transport minima, the SAF is pushed southwest, as the MC continues flowing towards the north to meet the BC, and performs a cyclonic loop flowing adjacent to the BCO (see fig. 12 of Artana *et al.*, 2016). Based on these intensity anomalies of the along-slope MC, two opposite regimes in the BMCZ, weak

and strong Malvinas, have been proposed (Ferrari *et al.*, 2017; Paniagua *et al.*, 2018): during the weak Malvinas regime, the MC retroflects, the inshore surface velocities are smaller, and the offshore velocities turn clockwise. As a consequence, over the slope, the SAF does not reach 41°S whereas the STF overshoots towards the southwest; the shift of the fronts generates positive SST anomalies (>4°C) over a large region near the STF at 40–41°S (Paniagua *et al.*, 2018). Conversely, during the strong Malvinas regime, the SAF and STF meet near 39°S along the slope, and the BCO breaks down as an isolated anticyclone. Moreover, Olguín Salinas *et al.* (2015) showed that the penetration of subtropical waters in the PCM due to a southward extension of the BC and a weakening of the MC shift the pattern of higher Chl-a values southwards. Thus, a more frequent and/or more persistent weak Malvinas-type regime during MIS 3 could explain both the SST_{50} positive anomalies and the enhanced primary productivity in the BMCZ, the western sector of the South Subtropical Convergence province.

Several authors have demonstrated the strengthening of the BC during periods of abrupt climate change during MIS 3. Based on SST reconstructions and the abundance of *G. bulloides*, Portilho-Ramos *et al.* (2015) and Pereira *et al.* (2018) recognized an increase in the Southern Brazil upwelling during MIS 3. According to these authors, there was a strengthening of the BC during Heinrich Stadials HS4 (40.2–38.3 ka BP) and HS3 (32.7–31.3 ka BP), in coincidence with the period of SST positive anomalies and enhanced primary productivity in the PCM (Fig. 9). The southernmost penetration of subtropical waters due to the strengthening of the BC and a more persistent and/or frequent weak Malvinas-type regime in the BMCZ could have given the perfect thermal stratification and nutrient conditions that favored the high primary productivity offshore the north PCM during MIS 3.

Changes in the Southern Ocean upwelling during MIS 3 could have also affected the nutrient availability in surface waters of the BMCZ. In the Southern Ocean, biogenic opal flux (BSi, an upwelling proxy) allowed to recognize a period of moderate enhancement of the wind-driven upwelling of the CDW south of the Polar Front during MIS 3. Relatively high BSi fluxes have been reconstructed both in the SE Atlantic sector of the Southern Ocean (Anderson *et al.*, 2009) and the Scotia Sea (Sprenk *et al.*, 2013), between 45–37.5 ka BP and between 39–32 ka BP, respectively (Fig. 9). Additionally, several studies have proposed an equatorward displacement of the northern SWW margin during glacial periods (Rojas *et al.*, 2009; Kaiser *et al.*, 2005). A poleward shift of the SWW during MIS 3 would generate a stronger upwelling in the Southern Ocean (Toggweiler *et al.*, 2006), enhancing the primary productivity south of the SAF (Anderson *et al.*, 2009). As part of the upwelled waters moved northwards at surface under the influence of the SWW, this would have enhanced the nutrient content of subantarctic surface waters carried by the MC to the BMCZ, boosting the primary productivity at the PCM. Additionally, as wind patterns south of the BMC are the main source of interannual variability at the latitude of separation of the BC (Garzoli & Giulivi, 1994), winds south of the BMC could affect not only the nutrient load carried by the MC but also the latitudinal position of the BCO, boosting or hindering the primary productivity in the BMCZ.

The frequent overshoot of the BC over the north PCM could also justify the observed changes in the phytoplankton community during MIS 3. Nowadays, the phytoplankton community in the patagonian shelfbreak during the warm season is composed of different key functional groups. Diatoms usually dominate numerically during spring before or right after the formation of the warm season thermocline, whereas coccolithophorids blooms occur during summer when nutrients are nearly consumed and the vertical stability enhances (García *et al.*, 2008; Sabatini *et al.*, 2012). This is because coccolithophores are well adapted not only to oligotrophic conditions but are often associated with well-stratified conditions (Litchman, 2007). Positive anomalies of the SST_{50} related to more frequent and/or persistent overshoots of the warmer, well-stratified BC would imply that the mixed layer became shallower and the thermocline stronger during MIS 3, constraining the nutrient input from sub-thermocline waters as occurred nowadays during summer conditions in the shelfbreak front, when coccolithophorid blooms take place.

As mentioned above, although several parameters provide solid evidence for enhanced primary productivity in the north PCM during MIS 3, benthic foraminifera-based indices do not indicate high surface productivity. The dominance of *U. peregrina* and the low contribution of the phytodetritus feeder *C. wuellestorfi* confirm the decoupling

of the pelagic and benthic communities. We attribute this finding to a very low POC export efficiency due to the small size of the dominant phytoplankton, as evidenced by the deposition of the calcareous muddy contourite facies composed mainly of calcareous nannoplankton. In addition, the dominance of *U. peregrina*, a species that has a clear diet preference for refractory organic matter (Jorissen & Wittling, 1999), highlights that partially degraded organic matter was more readily available than fresh phytodetritus at the sea bottom in the middle slope of the PCM. The lower-than-present sea level during MIS 3 (Grant *et al.*, 2012) that partly exposed the Patagonian shelf (Ponce *et al.*, 2011) could have potentially enhanced the terrigenous input from the outer shelf further offshore, providing an alternative source of food to the benthic communities.

CONCLUSIONS

In this study, we analyzed planktonic and benthic foraminifera assemblages from the sediment core AU_Geo02_GC20 (45° 55′ S; 58° 30′ W) retrieved from Patagonian Continental Margin (PCM), along with sedimentological data, to reconstruct surface and bottom conditions that prevailed in the area of the middle slope during MIS 3. We used a foraminifera-based multiproxy approach to assess changes in primary productivity and subsurface (50 m water depth) temperature and discuss changes in the nutrient availability in the Brazil Malvinas Confluence Zone (BMCZ) that occurred due to changes in the thermocline and nutricline depths.

Our results indicate a significant increase in primary productivity between 44–33.6 ka BP, which was accompanied by positive subsurface anomalies of ca. 2°C, indicating a shallowing of the thermocline. As strong mesoscale features characterize the BMCZ, we suggest that this period of enhanced primary productivity and positive SSTs anomalies in the north PCM reflects more frequent and/or persistent southward intrusions of the BC and blocking events of the MC south of 45°S.

The frequent overshoot of the BC over the north PCM can also explain the observed changes in the phytoplankton community during the last part of the MIS 3. The high primary productivity event between 43–36.3 ka BP coincides with the deposition of the calcareous muddy contourite facies, composed almost exclusively of calcareous nannoplankton. In the PCM, extensive blooms of the coccolithophores occur nowadays during summer, when surface waters are well stratified and the nutricline shallows. The dominance of the benthic foraminifera *Uvigerina peregrina*, which has diet preferences for refractory organic matter, and the low contribution of phytodetritus-feeder species such as *C. wuellestorfi*, suggest the decoupling of the pelagic and benthic foraminifera communities due to a low particulate organic carbon export efficiency of the cocco-lithophorid-dominated phytoplankton communities. In coincidence with the sandy-silty contourite facies deposition, an intense episode of carbonate dissolution characterizes the deposition of MIS 2 at the coring site.

ACKNOWLEDGEMENTS

This research was supported by the Consejo Nacional de Investigaciones Científicas y Técnicas (CONICET) (grant PIP11220150100038CO) and the Buenos Aires University (grant UBACyT 20020190100204BA) of Argentina. The core presented in this manuscript was acquired as part of a Pampa Azul subproject coined "YTEC-GTGM". The authors are also especially grateful to the captain, crew, and onboard scientific team for their support during the R/V Austral Geo02 cruise (Argentina) and the R/V SONNE SO260 cruise (MARUM, Germany). We are also grateful to Dr. Cristiano Mazur Chiessi (Universidade de São Paulo - Escola de Artes, Ciências e Humanidades, Brazil) and the FAPESP grant 2018/15123-4. The data reported in this paper is archived in Pangaea (https://doi.pangaea.de/10.1594/PANGAEA.949261). This is publication number R429 of the IDEAN (UBA-CONICET).

REFERENCES

Agosta Scarel, E. A., & Compagnucci, R. H. (2016). Abrupt climate changes during the Marine Isotope Stage 3 (MIS 3). In G. M. Gasparini, J. Rabassa, C. Deschamps, & E. P. Tonni (Eds.), *Marine Isotope Stage 3 in Southern South America, 60 ka BP-30 ka BP* (pp. 81–106). Springer Verlag.

Albarracín, P. B. (2021). *Reconstrucción de la productividad primaria durante el MIS 3 (Cuaternario Superior) en base a foraminíferos planctónicos en el Margen Patagónico.* (Tesis de Licenciatura, Facultad de Ciencias Exactas y Naturales, Universidad de Buenos Aires, Buenos Aires).

Alperín, M. I., Cusminsky, G. C., & Bernasconi, E. (2011). Benthic foraminiferal morphogroups on the Argentine continental shelf. *The Journal of Foraminiferal Research*, *41*(2), 155–166.

Anderson, R. F., Ali, S., Bradtmiller, L. I., Nielsen, S. H. H., Fleisher, M. Q., Anderson, B. E., & Burckle, L. H. (2009). Wind-driven upwelling in the Southern Ocean and the deglacial rise in atmospheric CO_2. *Science*, *323*(5920), 1443–1448.

Arhan, M., Heywood, K. J., & King, B. A. (1999). The deep waters from the Southern Ocean at the entry to the Argentine Basin. *Deep Sea Research Part II, 46*(1),475–499.

Arhan, M., Naveira Garabato, A. C., Heywood, K. J., & Stevens, D. P. (2002). The Antarctic Circumpolar Current between the Falkland Islands and South Georgia. *Journal of Physical Oceanography*, *32*, 1914–1931.

Artana, C., Ferrari, R., Koenig, Z., Saraceno, M., Piola, A. R., & Provost, C. (2016). Malvinas Current variability from Argo floats and

satellite altimetry. *Journal of Geophysical Research: Oceans*, *121*, 4854–4872.

Artana, C., Ferrari, R., Koenig, Z., Sennéchael, N., Saraceno, M., Piola, A. R., & Provost, C. (2018). Malvinas Current volume transport at 41°S: A 24 year long time series consistent with mooring data from 3 decades and satellite altimetry. *Journal of Geophysical Research: Oceans*, *123*, 378–398.

Artana, C., Provost, C., Poli, L., Ferrari, R., & Lellouche, J. M. (2021). Revisiting the Malvinas Current Upper Circulation and Water Masses Using a High-Resolution Ocean Reanalysis. *Journal of Geophysical Research: Oceans*, *126*, e2021JC017271. https://doi.org/10.1029/2021JC017271

Basov, I. A., Ciesielski, P. F., Krasheninnikov, V. A., Weaver, F. M., Wise, S. W., & Ludwig, W. J. (1983). Biostratigraphic and paleontologic synthesis: Deep Sea Drilling Project Leg 71, Falkland Plateau and Argentine Basin. *Initial Reports of the Deep Sea Drilling Project*, *71*, 445–460.

Berger, W. H., & Diester-Haas, L. (1988). Paleoproductivity: the benthic/planktonic ratio in foraminifera as a productivity index. *Marine Geology*, *81*(1–4), 15–25.

Bermúdez, P. J. (1961). Contribución al estudio de la Globigerinidea de la región Caribe-Antillana. *Memoria Tercer Congreso Geológico Venezolano. Special Publication*, *3*, 1119–1393.

Bernasconi, E., & Cusminsky, G. (2020). Calcareous microorganisms as indicators of oceanographic conditions in South West Atlantic Ocean. *Journal of Marine Systems*, *208*, 103369. https://doi.org/10.1016/j.jmarsys.2020.103369

Bernasconi, E., Cusminsky, G. C., & Gómez, E. A. (2009). Foraminíferos bentónicos del Holoceno del Golfo Nuevo, Argentina: inferencias paleoclimáticas. *Revista Española de Micropaleontología*, *41*(1–2), 21–34.

Bernasconi, E., Cusminsky, G., & Gordillo, S. (2019). Distribution of foraminifera from South Shetland Islands (Antarctic): Ecology and taphonomy. *Regional Studies in Marine Science*, *29*, 100653. https://doi.org/10.1016/j.rsma.2019.100653

Bernasconi, E., Mansilla, M., & Cusminsky, G. (2018). Recent benthic foraminifers from the South Atlantic shelf of Argentina. *Journal of Foraminiferal Research*, *48*(3), 210–222.

Bertels, A. (1987). Foraminíferos planctónicos del Neógeno del Océano Atlántico sudoccidental austral. *Revista Española de Micropaleontologia*, *17*(2), 221–252.

Bertels, A., & Núñez, H. J. (1989). Micropaleontología y paleomagnetismo de sedimentos del Océano Atlántico Sudoccidental Austral en el Neógeno: sus hiatos. *Revista Española de Micropaleontología*, *21*(3), 391–408.

Birks, H. J. B. (1995). Quantitative palaeoenvironmental reconstructions. In D. Maddy, & J. S. Brew (Eds.), *Statistical Modelling of Quaternary Science data. Technical guide, 5, Quaternary Research Association* (pp.161–254). Quaternary Research Association.

Birks, H. J. B., Braak, C. T., Line, J. M., Juggins, S., & Stevenson, A. C. (1990). Diatoms and pH reconstruction. *Philosophical transactions of the Royal Society of London. B, Biological Sciences*, *327*(1240), 263–278.

Blaauw, M. (2010). Methods and code for 'classical' age-modelling of radiocarbon sequences. *Quaternary Geochronology*, *5*(5), 512–518.

Boltovskoy, E., Giussani, G., Watanabe, S., & Wright, R. C. (1980). *Atlas of benthic shelf foraminifera of the southwest Atlantic*. Springer Science & Business Media.

Bostock, H. C., Prebble, J. G., Cortese, G., Hayward, B., Calvo, E., & Quirós-Collazos, L. (2019). Paleoproductivity in the SW Pacific Ocean during the early Holocene climatic optimum. *Paleoceanography and Paleoclimatology*, *34*, 580–599.

Bozzano, G., Cerredo, M. E., Remesal, M., Steinmann, L., Hanebut, T. J. J., Schwenk, T., Baqués, M., Hebbeln, D., Spoltore, D., Silvestri, O., Acevedo, R. D., Spiess, V., Violante, R. A., & Kasten, S. (2020). Dropstones in the Mar del Plata Canyon Area (SW Atlantic): Evidence for Provenance, Transport, Distribution, and Oceanographic Implications. *Geochemistry, Geophysics, Geosystems,22*, e2020GC009333. https://doi.org/10.1029/2020GC009333

Bozzano, G., Martín, J., Spoltore, D. V., & Violante, R. A. (2017). Los cañones submarinos del Margen Continental Argentino: una síntesis sobre su génesis y dinámica sedimentaria. *Latin American Journal of Sedimentology and Basin Analysis*, *24*(1), 85–101.

Bozzano, G., Violante, R. A., & Cerredo, M. E. (2011). Middle slope contourite deposits and associated sedimentary facies of NE Argentina. *Geo-Marine Letters*, *31*, 495–507.

Braconnot, P., Harrison, S. P., Kageyama, M., Bartlein, P. J., Masson-Delmotte, V., Abe-Ouchi, A., Otto-Bliesner, B., & Zhao, Y. (2012). Evaluation of climate models using palaeoclimatic data. *Nature Climate Change*, *2*(6), 417–424.

Brady, H. B. (1877). Supplementary note on the Foraminifera of the Chalk (?) of the New Britain Group. *Geological Magazine (Decade II)*, *4* (12), 534–536.

Brown, R. E., Anderson, L. D., Thomas, E., & Zachos, J. C. (2011). A core-top calibration of B/Ca in the benthic foraminifera *Nuttallides umbonifera* and *Oridorsalis umbonatus:* reconstructing bottom water carbonate saturation. *Earth and Planetary Science Letters*, *310*, 360–368.

Brummer, G. J. A., & Kucera, M. (2022). Taxonomic review of living planktonic foraminifera, *Journal of Micropalaeontology*, *41*, 29–74.

Butzin, M., Köhler, P., & Lohmann, G. (2017). Marine radiocarbon reservoir age simulations for the past 50,000 years. *Geophysical Research Letters*, *44*(16), 8473–8480.

Cai, P., Huang, Y., Chen, M., Liu, G., & Qiu, Y. (2002). New production in the South China Sea. *Science in China Series D: Earth Sciences*, *45*(2), 103–109.

Cao, Z., Dai, M., Evans, W., Gan, J., & Feely, R. (2014). Diagnosing CO_2 fluxes in the upwelling system off the Oregon–California coast. *Biogeosciences*, *11*(22), 6341–6354.

Carranza, M. M., Gille, S. T., Piola, A. R., Charo, M., & Romero, S. I. (2017). Wind modulation of upwelling at the shelf-break front off Patagonia: Observational evidence, *Journal Geophysical Research*: *Oceans*, *122* (3), 2401– 2421.

Cavallotto, J. L., Violante, R. A., & Hernández-Molina, F. J. (2011). Geological aspects and evolution of the Patagonian continental margin. *Biological Journal of the Linnean Society*, *103*(2), 346–362.

Cermeño, P., Dutkiewicz, S., Harris, R. P., Follows, M., Schofield, O., & Falkowski, P. G. (2008). The role of nutricline depth in regulating the ocean carbon cycle. *Proceedings of the National Academy of Sciences*, *105*(51), 20344–20349.

Ciais, P., Sabine, C., Bala, G., Bopp, L., Brovkin, V., Canadell, J., Chabra, A., De Fries, R., Galloway, J., Heimann, M., Jones, C., Le Quéré, C., Myneni, R. B., Piao, S., & Thornton, P. (2014). Carbon and other biogeochemical cycles. In T. F. Stocker, D. Qin, G.-K. Plattner, M. Tignor, S. K. Allen, J. Boschung, A., Nauels, Y. Xia, V., Bex, & P. M. Midgley (Eds.), *Climate Change 2013: the physical science basis. Contribution of Working Group I to the Fifth Assessment Report of the Intergovernmental Panel on Climate Change* (pp. 465–570). Cambridge University Press.

Cifelli, R. (1961). *Globigerina incompta*, a new species of pelagic foraminifera from the North Atlantic. *Contributions from the Cushman Laboratory for Foraminiferal Research*, *12*(3), 83–86.

Crundwell, M. P., Scott, G., Naish, T., & Carter, L. (2008). Glacial–interglacial ocean climate variability from planktonic foraminifera during the Mid-Pleistocene transition in the temperate

Southwest Pacific, ODP Site 1123. *Palaeogeography, Palaeoclimatology, Palaeoecology*, *260*, 202–229.

Curry, W. B., & Oppo, D. W. (2005). Glacial water mass geometry and the distribution of δ^{13} of ΣCO_2 in the western South Atlantic. *Paleoceanography 20*, PA1017. ttps://doi.org/10.1029/2004PA001021

Cushman, J. A. (1923). *The Foraminifera of the Atlantic Ocean. Part 4: Lagenidae*. Smithsonian Institution, United States National Museum Bulletin 104.

Cusminsky, G. C. (1991). Foraminíferos planctónicos de testigos cenozoicos del Océano Atlántico sudoccidental austral. *Ameghiniana*, *28*(3–4), 225–240.

Cusminsky, G. C. (1992). Foraminíferos bentónicos provenientes de testigos del océano Atlántico sudoccidental austral. *Revista Española de Micropaleontología*, *24*(1), 455–482.

Cusminsky, G. C. (1994). Estudio micropaleontológico (foraminíferos) de dos testigos provenientes del Océano Atlántico sudoccidental austral. *Revista Española de Micropaleontología*, *26*(2), 109–123.

Darling, K. F., Kucera, M., Kroon, D., & Wade, C. M. (2006). A resolution for the coiling direction paradox in *Neogloboquadrina pachyderma*. *Paleoceanography*, *21*, PA2011. https://doi.org/10.1029/2005PA001189

Dogliotti, A. I., Lutz, V. A., & Segura, V. (2014). Estimation of primary production in the southern Argentine continental shelf and shelf-break regions using field and remote sensing data. *Remote sensing of environment*, *140*, 497–508.

d'Orbigny, A. D. (1826). Tableau méthodique de la classe des Céphalopodes. *Annales des Sciences Naturelles*, *7*, 96–314.

d'Orbigny, A. D. (1839). Foraminifères. In M. R. de la Sagra (Ed.), *Histoire physique, politique et naturelle de l'Ile de Cuba* (pp. 1–224). A. Bertrand.

Duplessy, J. C., Shackleton, N. J., Fairbanks, R. G., Labeyrie, L., Oppo, D., & Kallel, N. (1988). Deepwater source variations during the last climatic cycle and their impact on the global deepwater circulation. *Paleoceanography*, *3*, 343–360.

Egger, J. G. (1893). Foraminiferen aus Meeresgrundproben, gelothet von 1874 bis 1876 von S.M. Sch. Gazelle. *Abhandlungen der Königlich Bayerischen Akademie der Wissenschaften, mathematisch-physikalische Klasse*, *18*(2), 193–458.

Ehrenberg, C. G. (1861). Elemente des tiefen Meeresgrundes in Mexikanischen Golfstrome bei Florida; Über die Tiefgrund-Verhältnisse des Oceans am Eingang der Davisstrasse und bei Island. *Monatsbericht der Koniglichen Preussischen Akademie der Wissenschaften zu Berlin*, 1861, 275–315.

Ewing, M., & Lonardi, A. G. (1971). Sediment transport and distribution in the Argentine Basin. 5. Sedimentary structure of the argentine margin, basin, and related provinces. *Physics and Chemistry of the Earth*, *8*, 125–156.

Eynaud, F. (2005). Planktonic foraminifera in the Arctic: potentials and issues regarding modern and quaternary populations. *IOP Conference Series: Earth and Environmental Science 14*: 012005. doi:10.1088/1755-1315/14/1/012005

Ferrari, R., Artana, C., Saraceno, M., Piola, A. R., & Provost, C. (2017). Satellite altimetry and current-meter velocities in the Malvinas Current at 41 S: Comparisons and modes of variations. *Journal of Geophysical Research: Oceans*, *122*(12), 9572–9590.

Franchito, S. H., Oda, T. O., Rao, V. B., & Kayano, M. T. (2008). Interaction between coastal upwelling and local winds at Cabo Frio, Brazil: an observational study. *Journal of Applied Meteorology and Climatology*, *47*(6), 1590–1598.

Friedlingstein, P. (2015). Carbon cycle feedbacks and future climate change. *Philosophical Transactions of the Royal Society A: Mathematical, Physical and Engineering Sciences*, *373*(2054), 20140421. https://doi.org/10.1098/rsta.2014.0421

García Chapori, N., & Kucera, M. (2019). Planktonic foraminifera census counts from the western South Atlantic. PANGAEA. doi:10.1594/PANGAEA.907931.

García Chapori, N., & Laprida, C. (2021). Planktonic foraminifera assemblages from the Brazil–Malvinas Confluence: palaeoceanographic implications of sub-surface temperature reconstructions in the western South Atlantic. *Lethaia*, *54*(4), 477–494.

García, C. A., Sarma, Y. V. B., Mata, M. M., & García, V. M. (2004). Chlorophyll variability and eddies in the Brazil–Malvinas Confluence region. *Deep Sea Research Part II: Topical Studies in Oceanography*, *51*(1–3), 159–172.

García, V. M., García, C. A., Mata, M. M., Pollery, R. C., Piola, A. R., Signorini, S. R., McClain, C. R., & Iglesias-Rodríguez, M. D. (2008). Environmental factors controlling the phytoplankton blooms at the Patagonia shelf-break in spring. *Deep Sea Research Part I: Oceanographic Research Papers*, *55*(9), 1150–1166.

Garzoli, S. L., & Giulivi, C. (1994). What forces the variability of the southwestern Atlantic boundary currents?. *Deep Sea Research Part I: Oceanographic Research Papers*, *41*(10), 1527–1550.

Gooday, A. J. (2003). Benthic foraminifera (Protista) as tools in deep-water palaeoceanography: Environmental influences on faunal characteristics. *Advances in Marine Biology*, *46*, 1–90.

Grant, K. M., Rohling, E. J., Bar-Matthews, M., Ayalon, A., Medina-Elizalde, M., Ramsey, C. B., Satow, C., & Roberts, A. P. (2012). Rapid coupling between ice volume and polar temperature over the past 150,000 years. *Nature*, *491*(7426), 744–747.

Gregg, W. W., Casey, N. W., & McClain, C. R. (2005). Recent trends in global ocean chlorophyll. *Geophysical Research Letters*, *32*(3), L03606. https://doi.org/10.1029/2004GL021808

Gruetzner, J., Uenzelmann-Neben, G., & Franke, D. (2012). Variations in sediment transport at the central Argentine continental margin during the Cenozoic. *Geochemistry, Geophysics, Geosystems*, *13*, 1–15.

Gupta, A. K., Das, M., Clemens, S. C., & Mukherjee, B. (2008). Benthic foraminiferal faunal and isotopic changes as recorded in Holocene sediments of the northwest Indian Ocean. *Paleoceanography*, *23*, PA2214. https://doi.org/10.1029/2007PA001546

Hales, B., Takahashi, T., & Bandstra, L. (2005). Atmospheric CO_2 uptake by a coastal upwelling system. *Global Biogeochemical Cycles*, *19*, GB1009. https://doi.org/10.1029/2004GB002295

Heiri, O., Lotter, A. F., & Lemcke, G. (2001). Loss on ignition as a method for estimating organic and carbonate content in sediments: reproducibility and comparability of results. *Journal of Paleolimnology*, *25*, 101–110.

Hemleben, C., Spindler, M., & Anderson, O. R. (1989). *Modern Planktonic Foraminifera.* Springer-Verlag.

Herguera, J. C. (1992). Deep-sea benthic foraminifera and biogenic opal: glacial to postglacial productivity changes in the western equatorial Pacific. *Marine Micropaleontology*, *19*(1–2), 79–98.

Herguera, J. C., & Berger, W. (1991). Paleoproductivity from benthic foraminifera abundance: Glacial to postglacial change in the west-equatorial Pacific. *Geology*, *19*(12), 1173–1176.

Hernández-Molina, F. J., Paterlini, M., Violante, R., Marshall, P., de Isasi, M., Somoza, L., & Rebesco, M. (2009). Contourite depositional system on the Argentine Slope: An exceptional record of the influence of Antarctic water masses. *Geology*, *37*(6), 507–510.

Hernández-Molina, F. J., Paterlini, C. M., Somoza, L., Violante, R. A., Arecco, M. A., de Isasi, M., Rebesco, M., Uenzelmann- Neben, G., Neben, S., & Marshall, P. (2010). Giant mounded drifts in the Argentina Continental Margin: Origins, and global implications

for the history of thermohaline circulation. *Marine and Petroleum Geology*, *27*, 1508–1530.

Isola, J., Bravo, M. E., Bozzano, G., Palma, F. I., Ormazábal, J. P., Principi, S., Spoltore, D., Martín, R., Esteban, F. D., & Tassone, A. A. (2021). The Late-Quaternary deposits of the Piedra Buena Terrace (Patagonian continental slope, SW Atlantic): An example of interaction between bottom currents and seafloor morphology. *Marine Geology*, *435*, 106459. https://doi.org/10.1016/j.margeo.2021.106459

Jorissen, F. J., & Wittling, I. (1999). Ecological evidence from live–dead comparisons of benthic foraminiferal faunas off Cape Blanc (Northwest Africa). *Palaeogeography, Palaeoclimatology, Palaeoecology*, *149*(1–4), 151–170.

Juggins, S. (2013). Quantitative reconstructions in palaeolimnology: new paradigm or sick science?. *Quaternary Science Reviews*, *64*, 20–32.

Kageyama, M., Braconnot, P., Harrison, S. P., Haywood, A. M., Jungclaus, J. H., Otto-Bliesner, B. L., Peterschmitt, J. Y., Abe-Ouchi, A., Albani, S., Bartlein, P. J., Brierley, C., Crucifix, M., Dolan, A., Fernández-Donado, L., Fischer, H., Hopcroft, P. O., Ivanovic, R. F., Lambert, F., Lunt, D. J., Mahowald, N. M., Peltier, W. R., Phipps, S. J., Roche, D. M., Schmidt, G. A., Tarasov, L., Valdes, P. J., Zhang, Q., & Zhou, T. (2018). The PMIP4 contribution to CMIP6–Part 1: Overview and over-arching analysis plan. *Geoscientific Model Development*, *11*(3), 1033–1057.

Kaiser, J., Lamy, F., & Hebbeln, D. (2005). A 70-kyr sea surface temperature record off southern Chile (Ocean Drilling Program Site 1233). *Paleoceanography*, *20*, PA4009. https://doi.org/10.1029/2005PA001146

Kennett, J. P., & Srinivasan, M. S. (1983). *Neogene Planktonic Foraminifera: a Phylogenetic Atlas.* Hutchinson Ross Publishing Company.

Kasten, S., Schwenk, T., Aromokeye, D., Baques, M., Baumann, K.-H., Bergenthal, M., Bösche, J., Bozzano, G., Brune, R., Bülten, J., Chiessi, C. M., Coffinet, S., Crivellari, S., Dehning, K., Dohrmann, I., Dröllner, M., Düßmann, R., Durica, J. T., Frederichs, T., García Chapori, N., Gonzalez, L., Hanebuth, T. J. J., Hilgenfeldt, C., Hüttich, D., Jones, C. K., Klann, M., Klar, S., Klein, T., Kockisch, B., Köster, M., Lantzsch, H., Linowski, E., Long, J. H., Melcher, A.-C., Ogunleye, O. J., Pereyra, N., Rehage, R., Riedinger, N., Rosiak, U., Schmidt, W., Schnakenberg, A., Spieß, V., Steinmann, L., Thieblemont, A., Volz, J., Warnke, F., Warratz, G., Wenau, S., & Zonneveld, K. A. F. (2019). Dynamics of sedimentation processes and their impact on biogeochemical reactions on the continental slope off Argentina and Uruguay (MARUM), Cruise No. SO260/Leg 1 & Leg 2, Leg 1: January 12 - January 30, 2018, Buenos Aires (Argentina) - Montevideo (Uruguay), Leg 2: February 2 - February, 14, 2018, Montevideo (Uruguay) - Buenos Aires (Argentina), DosProBio. doi: 10.2312/cr_so260.

Lastras, G., Acosta, J., Muñoz, A., & Canals, M. (2011). Submarine canyon formation and evolution in the Argentine Continental Margin between 44° 30′ S and 48° S. *Geomorphology*, *128*, 116–136.

Lessa, D., Morard, R., Jonkers, L., Venancio, I. M., Reuter, R., Baumeister, A., Albuquerque, A., & Kucera, M. (2019). Vertical distribution of planktonic foraminifera in the Subtropical South Atlantic: depth hierarchy of controlling factors. *Biogeosciences*, *17*, 4313–4342.

Lessa, D. V., Ramos, R. P., Barbosa, C. F., da Silva, A. R., Belem, A., Turcq, B., & Albuquerque, A. L. (2014). Planktonic foraminifera in the sediment of a western boundary upwelling system off Cabo Frio, Brazil. *Marine Micropaleontology*, *106*, 55–68.

Lisiecki, L. E., & Raymo, M. E. (2005). A Pliocene-Pleistocene stack of 57 globally distributed benthic delta^{18}O records. *Paleoceanography and Paleoclimatology*, *20*, PA1003. doi:10.1029/2004PA001071

Litchman, E. (2007). Resource Competition and the Ecological Success of Phytoplankton. In P. G. Falkowski, & A. H. Knoll (Eds.), *Evolution of Primary Producers in the Sea* (pp. 351–376). Elsevier.

Loeblich, A. R., & Tappan, H. (1988). *Foraminiferal genera and their classification*. Springer.

Locarnini, R. A., Mishonov, A. V., Antonov, J. I., Boyer, T. P., García, H. E., Baranova, O. K., Zweng, M. M., Paver, C. R., Reagan, J. R., Johnson, D. R., Hamilton, M., Seidov, D., & Levitus, S. (2013). Volume 1: Temperature. In S. Levitus, *World Ocean Atlas 2013* (pp. 1–40), NOAA Atlas NESDIS 73.

Lombard, F., Labeyrie, L., Michel, E., Bopp, L., Cortijo, E., Retailleau, S., Howa, H., & Jorissen, F. (2011). Modelling planktic foraminifer growth and distribution using an eco-physiological multispecies approach. *Biogeosciences*, *8*, 853–873.

Longhurst, A. (2006). *Ecological Geography of the Sea Second Edition.* Elsevier.

Lutz, V., Segura, V., Dogliotti, A., Gagliardini, D., Bianchi, A., & Balestrini, C. (2010). Primary production in the Argentine Sea during spring estimated by field and satellite models. *Journal of Plankton Research*, *32* (2), 181–195.

Lutz, V., Segura, V., Dogliotti, A., Tavano, V., Brandini, F. P., Calliari, D. L., Ciotti, A. M., Villafañe, V. F., Schloss, I. R., Saldanha Corrêa, F. M. P., Benavides, H., & Cantonnet, D. V. (2018). Overview on primary production in the Southwestern Atlantic. In M. S. Hoffmeyer, M. E. Sabatini, F. P. Brandini, D. L. Calliari, & N. H. Santinelli (Eds.), *Plankton Ecology of the Southwestern Atlantic: From the Subtropical to the Subantarctic Realm* (pp. 101–126). Springer International Publishing AG.

Marrari, M., Piola, A. R., & Valla, D. (2017). Variability and 20-year trends in satellite-derived surface chlorophyll concentrations in large marine ecosystems around South and Western Central America. *Frontiers in Marine Science*, *4*, 372. https://doi.org/10.3389/fmars.2017.00372

Matano, R. P., & Palma, E. D. (2008). On the upwelling of downwelling currents. *Journal of Physical Oceanography*, *38*(11), 2482–2500.

Menviel, L., Spence, P., & England, M. H. (2015). Contribution of enhanced Antarctic Bottom Water formation to Antarctic warm events and millennial-scale atmospheric CO_2 increase. *Earth and Planetary Science Letters*, *413*, 37–50.

Miller, R. N., Matano, R. P., & Palma, E. D. (2011). Shelfbreak upwelling induced by alongshore currents: analytical and numerical results. *Journal of Fluid Mechanics*, *686*, 239–249.

Morey, A. E., Mix, A. C., & Pisias, N. G. (2005). Planktonic foraminiferal assemblages preserved in surface sediments correspond to multiple environment variables. *Quaternary Science Reviews*, *24*(7–9), 925–950.

Mouw, C. B., Barnett, A., McKinley, G. A., Gloege, L., & Pilcher, D. (2016). Phytoplankton size impact on export flux in the global ocean. *Global Biogeochemical Cycles*, *30*, 1542–1562.

Mulitza, S., Paul, A., & Wefer, G. (2013). Late Pleistocene South Atlantic. In S.A. Elias (Ed.), *Encyclopedia of Quaternary Science* (pp. 1816–1831). Elsevier.

Murdmaa, I. O., Dara, O., Dorokhova, E., & Simagin, N. (2018). Glauconite sand from the terrace of the Patagonian Continental Slope, Southwestern Atlantic. *Lithology and Mineral Resources*, *53*, 455–459.

Nagai, T., Tandon, A., Gruber, N., & McWilliams, J. C. (2008). Biological and physical impacts of a geostrophic frontal circulations driven by confluent flow and vertical mixing. *Dynamics of Atmospheres and Oceans*, *45*, 229–251.

NASA. (2018). Goddard Space Flight Center, Ocean Ecology Laboratory, Ocean Biology Processing Group. Moderate-resolution Imaging Spectroradiometer (MODIS) Aqua Chlorophyll, POC and aph data. (2018). Reprocessing. NASA OB.DAAC, Greenbelt, MD, USA. https://oceancolor.gsfc.nasa.gov/data/10.5067/AQUA/MODIS/L3B/CHL/2018/ Accessed on 05/18/2022.

Natland, M. L. (1938). New species of foraminifera from off the west coast of North America and from the later Tertiary of the Los Angeles Basin. University of California, *Scripps Institution of Oceanography Bulletin, Technical Series*, *4* (5), 137–163.

Olguín Salinas, H. F., Brandini, F., & Boltovskoy, D. (2015). Latitudinal patterns and interannual variations of spring phytoplankton in relation to hydrographic conditions of the southwestern Atlantic Ocean (34–62° S). *Helgoland Marine Research*, *69*(2), 177–192.

Orsi, A. H., Whitworth, T., & Nowlin, W. D. (1995). On the meridional extent and fronts of the Antarctic Circumpolar Current. *Deep-Sea Research I*, *42*(5), 641–673.

Paniagua, G. F., Saraceno, M., Piola, A. R., Guerrero, R., Provost, C., Ferrari, R., Lago, L. S., & Artana, C. I. (2018). Malvinas Current at 40°S–41°S: First assessment of temperature and salinity temporal variability. *Journal of Geophysical Research: Oceans*, *123*(8), 5323–5340.

Parker, G., Violante, R. A., & Paterlini, C. M. (1996). Fisiografía de la plataforma continental. *Geología y recursos naturales de la Plataforma Continental Argentina*, *1*, 1–16.

Pereira, L. S., Arz, H. W., Paetzold, J., & Portilho-Ramos, R. C. (2018). Productivity evolution in the South Brazilian Bight during the last 40,000 years. *Paleoceanography and Paleoclimatology*, *33*(12), 1339–1356.

Piola, A. R., & Matano, R. P. (2001). The South Atlantic Western Boundary Currents Brazil/Falkland (Malvinas) Currents. In J. M. Steele, K. K. Turekian, & S. A. Thorpe (Eds.), *Encyclopedia of Ocean Sciences* (pp. 340–349). Elsevier Science Ltd.

Piola, A., & Falabella, V. (2009). El Mar Patagónico. In V. Falabella, C. Campagna, C., & J. Croxall (Eds.), *Atlas del Mar Patagónico. Especies y Espacios* (pp. 56–75). Wildlife Conservation Society and Birdlife International.

Piola, A. R., Palma, E. D., Bianchi, A. A., Castro, B. M., Dottori, M., Guerrero, R. A., & Saraceno, M. (2018). Physical oceanography of the SW Atlantic Shelf: a review. In M. S. Hoffmeyer, M. E. Sabatini, F. P. Brandini, D. L. Calliari, & N. H. Santinelli (Eds.), *Plankton ecology of the Southwestern Atlantic. From the Subtropical to the Subantarctic Real* (pp. 37–56). Springer International Publishing AG.

Ponce, J. F., Rabassa, J., Coronato, A., & Borromei, A. M. (2011). Palaeogeographical evolution of the Atlantic coast of Pampa and Patagonia from the last glacial maximum to the Middle Holocene. *Biological Journal of the Linnean Society*, *103*(2), 363–379.

Portilho-Ramos, R., Ferreira, F., Calado, L., Frontalini, F., & Toledo, M. (2015). Variability of the upwelling system in the southeastern Brazilian margin for the last 110,000 years. *Global and Planetary Change*, *135*, 179–189.

Portilho-Ramos, R. D. C., Pinho, T. M. L., Chiessi, C. M., & Barbosa, C. F. (2018). Understanding the mechanisms behind high glacial productivity in the southern Brazilian margin. *Climate of the Past*, *15*(3), 943–955.

Preu, B., Hernández-Molina, F. J., Violante, R., Piola, A. R., Paterlini, C. M., Schwenk, T., Voigt, I., Krastel, S., & Spieß, V. (2013). Morphosedimentary and hydrographic features of the northern Argentine margin: The interplay between erosive, depositional and gravitational processes and its conceptual implications. *Deep Sea Research*, *75*, 157–174.

Preu, B., Schwenk, T., Hernández Molina, F. J., Violante, R. A., Paterlini, C. M., Krastel, S., Tomasini, J., & Spieß, V. (2012). Sedimentary growth pattern on the northern Argentine slope: The impact of North Atlantic Deep Water on southern hemisphere slope architecture. *Marine Geology*, *329–331*,113–125.

R Core Team. (2018). R: A language and environment for statistical computing. R Foundation for Statistical Computing, Vienna, Austria. URL https://www.R-project.org/. Reimer, P., Austin, W., Bard, E., Bayliss, A., Blackwell, P., Bronk Ramsey, C., Butzin, M., Cheng, H., Lawrence Edwards, R., Friedrich, M., Grootes, P. M., Guilderson, T. P., Hajdas, I., Heaton, T. J., Hogg, A. G., Hughen, K. A., Kromer, B., Manning, S. W., Muscheler, R., Palmer, J. G., Pearson, C., van der Plicht, J., Reimer, R. W., Richards, D. A., Scott, E. M., Southon, J. R., Turney, C. S., Wacker, L., Adolphi, F., Büntgen, U., Capano, M., Fahrni, S. M., Fogtmann-Schulz, A., Friedrich, R., Köhler, P., Kudsk, S., Miyake, F., Olsen, J., Reinig, F., Sakamoto, M., Sookdeo, A., & Talamo, S. (2020). The IntCal20 Northern Hemisphere Radiocarbon Age Calibration Curve (0–55 cal kBP). *Radiocarbon*, *62*(4), 725–757.

Reuss, A. E. (1851). Über die fossilen Foraminiferen und Entomostraceen der Septarienthone der Umgegend von Berlin. *Zeitschrift der Deutschen Geologischen Gesellschaft*, *3*(1), 49–92.

Rivas, A. L., Dogliotti, A. I., & Gagliardini, D. A. (2006). Seasonal variability in satellite-measured surface chlorophyll in the Patagonian Shelf. *Continental Shelf Research*, *26*, 703–720.

Roberts, J., McCave, I. N., McClymont, E. L., Kender, S., Hillenbrand, C. D., Matano, R., Hodell, D. A., & Peck, V. L. (2017). Deglacial changes in flow and frontal structure through the Drake Passage. *Earth and Planetary Science Letters*, *474*, 397–408.

Rojas, M., Moreno, P. I., Kageyama, M., Crucifix, M., Hewitt, C., Abe-Ouchi, A., Ohgaito, R., Brady, E. C., & Hope, P. (2009). The Southern Westerlies during the last glacial maximum in PMIP2 simulations. *Climate Dynamics*, *32* (4), 525–548.

Romero, S. I., Piola, A. R., Charo, M., & García, C. A. E. (2006). Chlorophyll-a variability off Patagonia based on SeaWiFS data. *Journal of Geophysical Research*, *111*, C05021. doi: 10.1029/2005JC003244

Sabatini, M. E., Akselman, R., Reta, R., Negri, R. M., Lutz, V. A., Silva, R. I., Segura, V., Gil, M. N., Santinelli, N. H., Sastre, A. V., Daponte, M. C., & Antacli, J. C. (2012). Spring plankton communities in the southern Patagonian shelf: hydrography, mesozooplankton patterns and trophic relationships. *Journal of Marine System*, *94*, 33–51.

Saraceno, M., Provost, C., & Piola, A. R. (2005). On the relationship between satellite-retrieved surface temperature fronts and chlorophyll-a in the western South Atlantic. *Journal of Geophysical Research: Oceans*, *110*, C11016. https://doi.org/10.1029/2004JC002736

Sarmiento, J. L., Slater, R., Barber, R., Bopp, L., Doney, S. C., Hirst, A. C., Kleypas, J., Matear, R., Mikolajewicz, U., Monfray, P., Soldatov, V., Spall, S. A., & Stouffer, R. (2004). Response of ocean ecosystems to climate warming. *Global Biogeochemical Cycles*, *18*, GB3003. https://doi.org/10.1029/2003GB002134

Schiebel, R., Waniek, J., Bork, M., & Hemleben, C. (2001). Planktic foraminiferal production stimulated by chlorophyll redistribution and entrainment of nutrients. *Deep-Sea Research I*, *48*(3), 721–740.

Schneider, B., Bopp, L., Gehlen, M., Segschneider, J., Frolicher, T. L., Joos, F., Cadule, P., Friedlingstein, P., Doney, S. C., & Behrenfeld, M. J. (2007). Spatio-temporal variability of marine primary and export production in three global coupled climate-carbon cycle models. *Biogeosciences Discussions*, *4*(3), 1877–1921.

Schwager, C. (1866). Fossile Foraminiferen von Kar Nikobar. Reise der Österreichischen Fregatte Novara um die Erde in den Jahren 1857, 1858, 1859 unter den Befehlen des Commodore B. von Wüllerstorf-Urbair. *Geologischer Theil (Zweite Abtheilung, Paläontologische Mittheilungen) 2*(2), 187–268.

Siccha, M., & Kucera, M. (2017). ForCenS, a curated database of planktonic foraminifera census counts in marine surface sediment samples. *Scientific Data*, *4*, 170109.

Sprenk, D., Weber, M. E., Kuhn, G., Rosén, P., Molina-Kescher, M., Liebetrau, V., & Röhling, H. G. (2013). Southern Ocean bioproductivity during the last glacial cycle-new detection method and decadal-scale insight from the Scotia Sea. In M. Hambrey, P. Barker, P. Barrett, V. Bowman, B. Davies, J. Smellie, & M. Tranter (Eds.), *Antarctic Palaeoenvironments and Earth-Surface Processes* (pp. 245–261). Special Publication of the Geological Society.

Steinmann, L., Baques, M., Wenau, S., Schwenk, T., Spiess, V., Piola, A. R., Bozzano, G., Violante, R., & Kasten, S. (2020). Discovery of a giant cold-water coral mound province along the northern Argentine margin and its link to the regional Contourite Depositional System and oceanographic setting. *Marine Geology*, *427*, 106223. https://doi.org/10.1016/j.margeo.2020.106223

Tsuchiya, M., Talley, L. D., & McCartney, M. S. (1994). Water mass distributions in the western South Atlantic: A section from South Georgia Island (54°S) northward across the equator. *Journal of Marine Research*, *52*, 55–81.

Toggweiler, J. R., Russell, J. L., & Carson, S. R. (2006). Midlatitude westerlies, atmospheric CO_2 and climate change during the ice ages. *Paleoceanography*, *21*(2), PA2005. https://doi.org/10.1029/2005PA001154

Valla, D., & Piola, A. (2015). Evidence of upwelling events at the northern Patagonian shelf break. *Journal of Geophysical Research: Oceans*, *120*, 7635–7656.

Valla, D., Piola, A. R., Meinen, C. S., & Campos, E. (2018). Strong mixing and recirculation in the northwestern Argentine Basin. *Journal of Geophysical Research: Oceans*, *123*, 4624– 4648.

Violante, R. A., Cavallotto, J. L., Bozzano, G., & Spoltore, D. (2017). Sedimentación marina profunda en el margen Continental Argentino: revisión y estado del conocimiento. *Latin American journal of Sedimentology and Basin Analysis*, *24*, 7–29.

Violante, R. A., Paterlini, C. M., Marcolini, S. I., Costa, I. P., Cavallotto, J. L., Laprida, C., Dragani, W., García Chapori, N., Watanabe, S., Totah, V., Rovere, E., & Osterrieth, M. L. (2014). The Argentine continental shelf: morphology, sediments, processes and evolution since the Last Glacial Maximum. In F. L. Chiocci, & A. R. Rivas (Eds.), *Continental shelves of the world: their evolution during the last glacio-eustatic cycle* (pp. 55–68). Geological Society Memoir, 41. The Geological Society of London.

Warratz, G., Henrich, R., Voigt, I., Chiessi, C. M., Kuhn, G., & Lantzsch, H. (2017). Deglacial changes in the strength of deep southern component water and sediment supply at the Argentine continental margin. *Paleoceanography*, *32*, 796–812.

Warratz, G., Schwenk, T., Voigt, I., Bozzano, G., Henrich, R., Violante, R., & Lantzsch, H. (2019). Interaction of a deep-sea current with a blind submarine canyon (Mar del Plata Canyon, Argentina). *Marine Geology*, 417, 106002. https://doi.org/10.1016/j.margeo.2019.106002

Wilckens, H., Miramontes, E., Schwenk, T., Artana, C., Zhang, W., Piola, A., Baques, M., Provost, C., Hernández-Molina, F. J., Felgendreher, M., Spiess, V., & Kasten, S. (2021). The erosive power of the Malvinas Current: Influence of bottom currents on morpho-sedimentary features along the northern Argentine margin (SW Atlantic Ocean). *Marine Geology*, *439*, 106539. https://doi.org/10.1016/j.margeo.2021.106539

Zuur, A. F., Ieno, E. N., & Smith, G. M. (2007). *Analyzing Ecological Data*. Springer-Verlag.

Zweng, M. M., Reagan, J. R., Antonov, J. I., Locarnini, R. A., Mishonov, A. V., Boyer, T. P., García, H. E., Baranova, O. K., Johnson, D. R., Seidov, D., & Biddle, M. M. (2013). Volume 2: Salinity. In S. Levitus (Ed.), *World Ocean Atlas 2013* (pp. 1–39 pp). NOAA Atlas NESDIS 74.

doi: 10.5710/AMGH.04.04.2023.3515

Submitted: 6 June 2022
Accepted: 4 April 2023
Published: xxxxxxxxxxxxx